

JOEL KUUSK

Measurement of top-of-canopy
spectral reflectance of forests
for developing vegetation
radiative transfer models



TARTU UNIVERSITY PRESS

This study was carried out at the Tartu Observatory, Estonia.

The dissertation was admitted on 10 June 2011 in partial fulfilment of the requirements for the degree of Doctor of Philosophy in physics (applied physics), and allowed for defense by the Council of the Institute of Physics, University of Tartu.

Supervisors: DSc Andres Kuusk, Tartu Observatory, Estonia
PhD Mart Noorma, University of Tartu, Estonia

Opponents: PhD Jouni Peltoniemi, Finnish Geodetic Institute, Finland
PhD Tarmo Kõuts, Institute of Marine Systems,
Tallinn University of Technology, Estonia

Defense: University of Tartu, Estonia, Scientific Council room
in the university main building, Ülikooli 18,
on 24 August 2011 at 14:15.

Publication of this thesis is granted by the Institute of Physics, University of Tartu and by the Doctoral School of Earth Sciences and Ecology created under the auspices of European Social Fund.



European Union
European Social Fund



Investing in your future

ISSN 1406-0647

ISBN 978-9949-19-730-9 (trükis)

ISBN 978-9949-19-731-6 (PDF)

Autoriõigus Joel Kuusk, 2011

Tartu Ülikooli Kirjastus

www.tyk.ee

Tellimus nr. 423

CONTENTS

LIST OF ORIGINAL PUBLICATIONS	6
LIST OF ACRONYMS	7
1 INTRODUCTION.....	9
1.1 Objectives	12
2 UAVSPEC-SERIES SPECTROMETER SYSTEMS.....	13
2.1 UAVSpec	14
2.2 UAVSpec2.....	16
2.3 UAVSpec3.....	18
2.4 UAVSpec4SWIR.....	18
3 CHARACTERISATION OF THE SPECTROMETERS	19
3.1 Dark signal temperature dependence	19
3.2 Instrument function	22
4 FIELD MEASUREMENTS	27
4.1 Calculation of reflectance factor	28
5 RESULTS AND DISCUSSION	30
5.1 A dataset for the validation of reflectance models.....	30
5.2 Vicarious calibration of satellite sensors.....	31
5.3 Comparison of measurements at different years.....	34
5.4 Comparison of simulations and measurements.....	36
SUMMARY	40
REFERENCES	43
SUMMARY IN ESTONIAN	48
ACKNOWLEDGMENTS	50
PUBLICATIONS	51

LIST OF ORIGINAL PUBLICATIONS

This thesis is based on the following papers, which are referred to in the text by their Roman numerals. The papers are reprinted with the kind permission from the publishers.

- I** J. Kuusk and A. Kuusk, “Autonomous lightweight airborne spectrometers for ground reflectance measurements”, in *Proceedings of the 2nd Workshop on Hyperspectral Image and Signal Processing: Evolution in Remote Sensing (WHISPERS 2010)*, Reykjavik, Iceland: IEEE, 14–16 June 2010.
- II** J. Kuusk, “Dark signal temperature dependence correction method for miniature spectrometer modules”, *Journal of Sensors*, vol. 2011, no. 608157, pp. 1–9, 2011.
- III** A. Kuusk, J. Kuusk, and M. Lang, “A dataset for the validation of reflectance models”, *Remote Sensing of Environment*, vol. 113, no. 5, pp. 889–892, 2009.
- IV** A. Kuusk, J. Kuusk, M. Lang, and T. Lökk, “Vicarious calibration of the PROBA/CHRIS imaging spectrometer”, *The Photogrammetric Journal of Finland*, vol. 22, no. 1, pp. 46–59, 2010.
- V** J. Kuusk, A. Kuusk, M. Lang, and A. Kallis, “Hyperspectral reflectance of boreo-nemoral forests in a dry and normal summer”, *International Journal of Remote Sensing*, vol. 31, no. 1, pp. 159–175, 2010.
- VI** A. Kuusk, T. Nilson, J. Kuusk, and M. Lang, “Reflectance spectra of RAMI forest stands in Estonia : simulations and measurements”, *Remote Sensing of Environment*, vol. 114, no. 12, pp. 2962–2969, 2010.

Author contributions:

- I** J. Kuusk had the leading role in designing and building the instrument, and writing the paper.
- II** J. Kuusk was the single author.
- III** J. Kuusk measured and processed the top-of-canopy and understory directional spectral reflectance data.
- IV** J. Kuusk measured and processed the top-of-canopy directional spectral reflectance data.
- V** J. Kuusk carried out the measurements, made the data analysis, and was the lead author in writing the paper.
- VI** J. Kuusk measured and processed the top-of-canopy and understory directional spectral reflectance data.

LIST OF ACRONYMS

8S2P	2 groups of 8 elements in series, connected in parallel
ACRM	A two-layer Canopy Reflectance Model
ADC	analog-to-digital converter
agl	above ground level
AHRS	attitude and heading reference system
AHS	Airborne Hyperspectral Scanner
AISA	Airborne Hyperspectral Imaging System
AOT	aerosol optical thickness
ASD	Analytical Spectral Devices Inc.
AVIRIS	Airborne Visible/Infrared Imaging Spectrometer
BRDF	bidirectional reflectance distribution function
BRF	bidirectional reflectance factor
CASI	Compact Airborne Spectrographic Imager
CHRIS	Compact High Resolution Imaging Spectrometer
DBH	diameter at breast height
DC	direct current
DD	degree day
DN	digital number
FEE	front-end-electronics
FOV	field-of-view
FRT	Forest Radiative Transfer
FWHM	full width at half maximum
GIS	geographic information system
GPS	global positioning system
iFOV	instantaneous field-of-view
InGaAs	indium gallium arsenide
LAI	leaf area index
LiPo	lithium-ion polymer
LOMO	Leningrad Optical Mechanical Amalgamation (Ленинградское оптико-механическое объединение)
MAS	Multi-Angle Spectrometer
MMS-1	Monolithic Miniature Spectrometer 1
MODIS	Moderate Resolution Imaging Spectroradiometer

NiCd	nickel-cadmium
NiMh	nickel-metal hydride
NIR	near-infrared
PARABOLA	Portable Apparatus for Rapid Acquisition of Bi-directional Observation of the Land and Atmosphere
PC	personal computer
NIR-PGS-1.7	Near-Infrared Plane Grating Spectrometer 1.7
PI	proportional-integrational
PROBA	Project for On Board Autonomy
PSF	point spread function
RAMI	RAdiation transfer Model Intercomparison
RC	radio controlled
RCR	remote cosine receptor
RMSE	root mean square error
SBC	single-board computer
Si	silicon
TOA	top-of-atmosphere
TOC	top-of-canopy
UAV	unmanned aerial vehicle
USB	universal serial bus
VALERI	VALidation of Land European Remote sensing Instruments
VNA	view nadir angle
VNIR	visible and near-infrared

I INTRODUCTION

Beginning of the satellite era in the second half of the 20th century introduced unprecedented opportunities for remote sensing. Earth observation satellites can provide global coverage and easy repetition of measurements. They record electromagnetic radiation that is either reflected or radiated from the Earth.

One of the key targets of remote sensing has always been vegetation since it influences the whole ecosystem and climate [1, 2]. While some parameters, e.g. area covered by vegetation, can be easily estimated from multispectral satellite imagery, deeper knowledge of radiative transfer in vegetation is needed for more detailed analysis of remotely sensed data [3]. Radiative transfer models represent our perception of photon transport in vegetation canopies. By comparing modelled and measured data, it is possible to validate and enhance the models, and thereby improve our knowledge of radiative transfer in vegetation. Theoretical background forms the basis of interpretation of remotely sensed data.

If a model can predict the reflectance factor of a target covered with vegetation having certain set of known properties, it can be used for solving the inverse problem i.e. estimating some parameters of the target based on the reflected signal measured by a sensor. By analyzing a satellite image, conclusions can be drawn for a very large area at once.

Vegetation radiative transfer models predict the top-of-canopy (TOC) reflectance factor. Satellites measure the top-of-atmosphere (TOA) radiance. In order that these quantities are comparable, the effect of the atmosphere must be removed. Atmospheric radiative transfer models can be used for translating the TOA radiance to the TOC radiance. If the TOC irradiance, which can be either measured directly or modelled with an atmospheric radiative transfer model, is known, the TOC reflectance can be calculated and compared to the modelled values. If the measured TOC reflectance spectra is available, these data can be used for verifying the quality of atmospheric correction of a satellite image.

Opportunities for calibrating satellite sensors after launch are scarce. Airborne and land-based instruments, on the other hand, can be taken to laboratory for frequent recalibration. Hence, the TOC reflectance measurements can be used for estimating the quality of the satellite sensor calibration. If the TOC reflectances are measured at a few locations, these can be related to the corresponding pixels of the satellite image and the resultant calibration coefficients can be extrapolated to the whole image [IV].

With increasing spectral and spatial resolution of the state-of-the-art satellite sensors, spatial coverage decreases. For being able to provide reasonably good temporal resolution for any given location on ground, modern satellites are capable of taking off-nadir images. Directional reflectance anisotropy is a fundamental property of nature. Observed reflectance factor varies with illumination and view-

ing angles [4–8]. In order that two satellite images can be compared, the difference of reflectance factors corresponding to the respective illumination and observation geometries must be known. Radiative transfer models can be used for adapting different images to each other.

Availability of the measured TOC reflectance spectra of forest stands is scarce. It is expensive and complicated to lift the instruments above a forest. There have been numerous measurements with sensors like Compact Airborne Spectrographic Imager (CASI) [9], Airborne Hyperspectral Imaging System (AISA) [10], Airborne Visible/Infrared Imaging Spectrometer (AVIRIS) [11], Airborne Hyperspectral Scanner (AHS) [12], etc. from aircrafts flying at altitudes from 500 m up to several kilometers above ground level (agl). Measurements made so high above the target need also atmospheric correction. Sensors like Portable Apparatus for Rapid Acquisition of Bi-directional Observation of the Land and Atmosphere (PARABOLA) [13] or Multi-Angle Spectrometer (MAS) [14] have been used for the TOC measurements from towers that are higher than the trees, but that sort of fixed instruments have very limited spatial coverage.

Industrial spectrometers have several limitations. They have been designed to satisfy the most common needs of different customers. However, for a specific task they are often not very easy to adapt. Industrial spectrometers tend to be too big and heavy, and not meant for working in harsh conditions. Often an operator's intervention is necessary. The airborne measurements need to be synchronized with the global positioning system (GPS) data and preferably with some imagery for visual verification of the targets. Imaging spectrometers are available which provide themselves hyperspectral imagery but they need extremely good, hence, expensive attitude and heading reference system (AHRS) for geocorrection.

Reflectance of grasses or field crops can be measured from a land-based platform. For obtaining representative sample of forest reflectances, the only possible way is lifting the instruments above the canopy. The easiest way for this may be an aerostat, but this is also the most limited option. Its stability is strongly affected by the wind and moving around above the forest is virtually impossible. Airplanes are much more suitable carriers. They are more stable, controllable, and can cover extensive areas. However, airplane needs a runway, which usually is not available in a forest. The best alternative is a helicopter. It can hover above a single target or fly over the whole test area. A helicopter can land in a clearing or nearby field for attaching and removing the instruments.

With the emergence of miniature spectrometer modules, designing very small and light spectrometer systems became possible. Using a 400 kg aircraft for carrying a 4 kg instrument is unreasonable use of resources. This brings to mind using some smaller and more cost-effective platform with similar capabilities. Natural choice would be a miniature helicopter.

A variety of miniature helicopters for radio controlled (RC) model hobbyists are available on the market. They are fairly cheap, but unfortunately they bare a major downside. Piloting a RC model helicopter is an extremely complicated task that takes years of practicing to master. Besides, manual control of a RC helicopter is limited to the visual range and therefore is impossible over forests.

Fortunately, few recent years have brought to market affordable yet reliable autopilots for model helicopters. They tremendously expand the capabilities of a RC helicopter, making it a full-featured unmanned aerial vehicle (UAV) out of a RC toy. Autopilots not only take the burden of keeping the helicopter flying and stable off the pilots shoulders, but allow operating it far beyond the visual range. Following preprogrammed GPS waypoints, an UAV can make a fully autonomous flight carrying instruments above the forest.

UAVs have some more advantages over manned aircrafts. First, operating them is more versatile and can adapt to rapidly changing weather conditions. Piloted helicopter can respond in a matter of hours. Using an UAV could reduce the response time to less than an hour and make the measurement independent of any service provider. This would allow to take most out of the very limited climatic conditions in the northern part of the temperate climate zone, suitable for reliable ground reflectance measurements.

Second, UAVs can fly at lower altitudes above the forest than is allowed for manned aircrafts by aviation regulations. This means that the layer of atmosphere between the target and the sensor is thinner.

Third, since aircrafts can have lateral ground speed, the magnetic field of the Earth is the most commonly used anchor for obtaining true heading of the aircraft, and consequently, the instruments. Since vegetation is anisotropic medium the reflectance values depend on illumination and view geometry. For off-nadir measurements it is important to know the exact view azimuth. A helicopter always contains some amount of ferromagnetic material that warps the Earth's magnetic field. This causes deviation of the compass reading. Since the ferromagnetic material does not move relative to the compass, its influence can be removed with a proper calibration procedure. As the attitude angles of the aircraft can change in rather wide range, a full three-dimensional calibration is necessary. This, however, requires rotating the compass together with all the disturbing ferromagnetic material around all three axes [15]. It is impossible with a piloted helicopter but feasible with an UAV.

This led to the decision to use an UAV as a carrier for a fully autonomous spectrometer system. Since there are no suitable instruments on the market, a miniature spectrometer module was chosen as the core of the spectrometer system and it was integrated with other necessary components in order to design an instrument suitable for measuring spectral directional reflectance factor of forests.

I.1 Objectives

The general aim of this study was providing the TOC measurements of forest spectral directional reflectance for validation of vegetation radiative transfer models. The specific aims were:

- Designing an autonomous spectrometer system suitable for measuring the TOC reflectance of forests from a lightweight carrier, such as an UAV [I].
- Studying and parameterizing the metrological properties of the spectrometer [II].
- Providing an exhaustive dataset for validation of the vegetation radiative transfer models [III].
- Proposing a workflow for vicarious calibration of satellite sensors based on the measured TOC spectral reflectance of forests [IV].
- Measuring and studying the short term variations of the TOC spectral reflectance of mature forest stands [V].
- Validating the Forest Radiative Transfer (FRT) model [16] [VI].

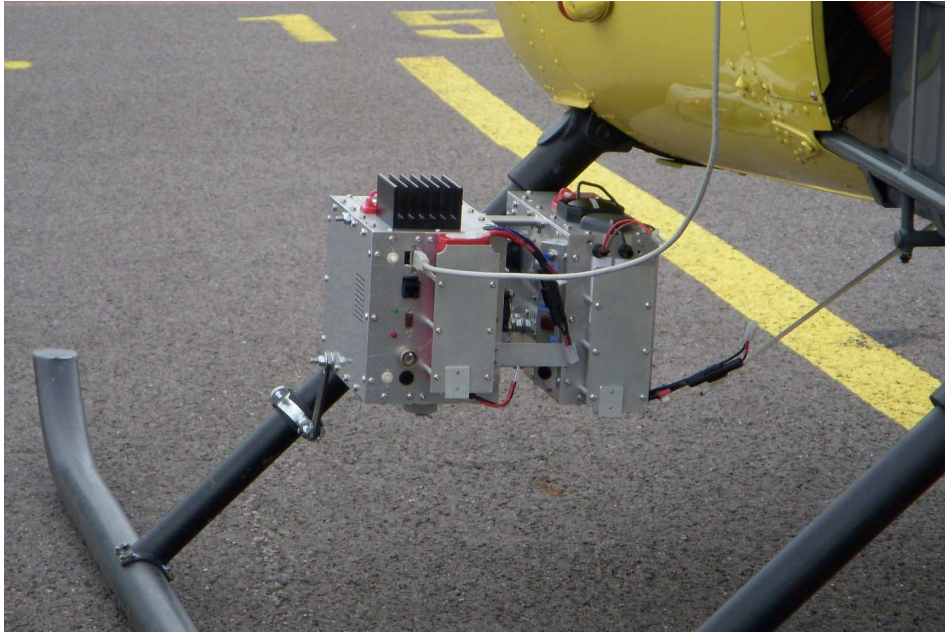


Figure 1. UAVSpec4SWIR (left) and UAVSpec3 (right) attached to the frame of a Robinson R22 helicopter.

2 UAVSPEC-SERIES SPECTROMETER SYSTEMS

The UAVSpec-series spectrometer systems were designed at the Tartu Observatory for measuring the TOC spectral reflectance of forests from an UAV platform [I]. The instruments are fully autonomous and do not need any operator's intervention during the flight. They are turned on before the flight and data is recorded continuously during the flight. The UAVSpec-series spectrometer systems have been used for the field measurements since 2006 [III, IV, V, VI, 17]. During these measurements a Robinson R22 helicopter was used for carrying the instruments (Fig. 1). There have not been any field measurements from the UAV platform due to technical problems with it. However, the first test flights of UAVSpec3 onboard an UAV have been carried out (Fig. 2).

Spectrometers designed for airborne measurements must have relatively rugged construction to cope with the vibrations of the aircraft and possible shocks during landing. Considering this limitation the UAVSpec-series spectrometer systems were designed without mechanical shutters to minimize the amount of moving parts. This adds some metrological problems, e.g. the dark signal measurements can not be made during the flight but only before and after the flight on the ground. Therefore, it is essential to have comprehensive understanding about the



Figure 2. UAVSpec3 and an UAV.

effect of different parameters, e.g. temperature and integration time, to the dark signal.

The miniature spectrometer modules have fiber optic inputs. This makes it possible to use the UAVSpec-series instruments in various situations. The spectrometers can be connected to an integrating sphere for leaf level measurements, equipped with different field-of-view (FOV) restrictors for canopy level acquisitions, or connected to a remote cosine receptor (RCR) for irradiance measurements.

The main parameters of the four UAVSpec-series spectrometer systems are listed in Table 1, block diagram of the hardware can be seen in Fig. 3.

2.1 UAVSpec

UAVSpec was the first of the series and was used for field measurements in 2006 [IV, V]. It was based on the 256-band near-infrared (NIR) enhanced version of the miniature spectrometer module Monolithic Miniature Spectrometer 1 (MMS-1) manufactured by Carl Zeiss Jena GmbH, with the front-end-electronics (FEE) board FEE-HS by Tec5 AG. The MMS-1 spectrometer module is built around a solid glass body. The concave imaging grating and the 256-band silicon (Si) linear sensor array are steadily attached to the glass body. The spectrometer has a fiber

Table 1. The main parameters of the UAVSpec-series spectrometer systems.

Device	UAVSpec	UAVSpec2	UAVSpec3	UAVSpec4SWIR
Spectrometer	MMS-1 NIR enhanced			PGS-NIR-1.7
Serial number	028582			047934
Detector	Si			cooled InGaAs
Spectral range	306 to 1140 nm			949 to 1701 nm
Number of pixels	256			256
Spectral resolution	10 nm			10 nm
Spectral step	3.3 nm			3 nm
ADC resolution	15 bit			15 bit
FEE	FEE-HS			FEE-1M
Integration time, ms	2 to 1000	60 to 5000	60 to 65 535	60 to 65 535
Dimensions, mm	170x80x130 +laptop +GPS receiver +battery	240x109x189	282x109x189	248x148x215
Weight	>4 kg	2.9 kg	2.6 kg	3.2 kg
Battery life	<4 h	≈1.5 h	>2 h	>3 h

optic input with a cross-section converter — single fibers of the fiber bundle in a linear configuration form the entrance slit [18]. A preamplifier is integrated with the spectrometer module. The FEE includes an analog-to-digital converter (ADC) and timing electronics for sensor readout [19]. The MMS-1 together with the FEE have 15 bit radiometric resolution, the noise level is about 2 to 3 bit.

Low-level control of the spectrometer was handled by custom-designed controller electronics. It functioned as an interface between the laptop personal computer (PC) and the FEE. It controlled the integration time of the sensor and monitored the battery voltage. It also measured the temperature with two thermistors. One of them was attached to the body of the MMS-1, the other one was glued to the ADC integrated circuit on the FEE. The controller board had a universal serial bus (USB) interface for communicating with the high-level control hardware. +5 V direct current (DC) power was drawn from the USB bus, ± 12 V required by the FEE was provided by an external +12 V nickel-cadmium (NiCd) battery and a DC/DC converter.

The high-level control program of the spectrometer system was running on a laptop PC with a Linux operating system. It gathered the data from the spectrometer, a Magellan SporTrak Pro GPS receiver, and a Logitech QuickCam Messenger web camera. The GPS and web camera data were used for georeferencing the measured spectra. The web camera images and GPS data were recorded approximately once per second. Due to technical reasons concerning the USB bus and

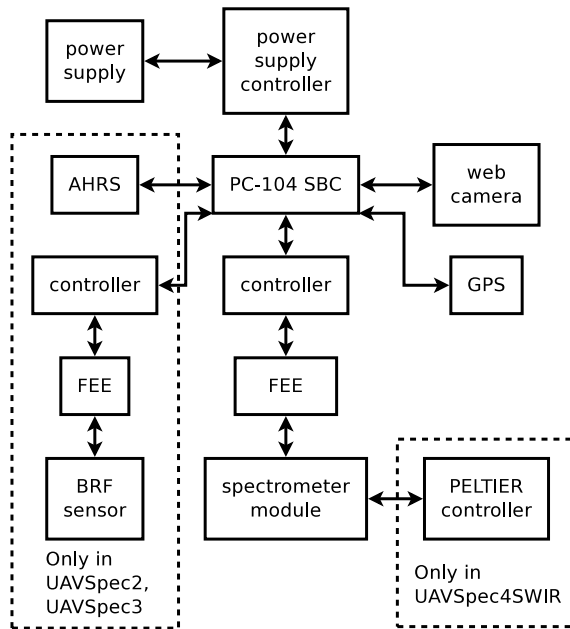


Figure 3. Block diagram of the hardware of the UAVSpec-series spectrometer systems.

sensor readout timings, quite significant amount of the spectral measurements had to be discarded. About 3 to 5 readings per second were stored in case of 120 ms integration time.

UAVSpec was the first development version of the UAVSpec-series spectrometer systems. It was never meant to be carried by an UAV, hence the use of a relatively large and heavy laptop PC.

During field measurements the foreoptics limited the FOV to 2° . Similar foreoptics was used for all the spectrometers during the TOC reflectance measurements.

2.2 UAVSpec2

UAVSpec2 was the next generation spectrometer system which was used for the field measurements in 2007 [III, V, VI]. The spectrometer module and FEE were exactly the same as in the UAVSpec, but everything else was new. The GPS receiver and web camera were replaced with smaller and more accurate Globalsat BU-353 (with SiRF Star III chipset) and Philips SPC-900NC, respectively. Instead of a Laptop PC, a PC/104-Plus single-board computer (SBC) Puma by VersaLogic Corporation Ltd. was used as the high-level controlling computer. The software and acquired data were stored at a Compact Flash card. The controller

between the FEE and SBC was new and instead of USB it used the RS-485 interface. This allowed to store more spectral measurements and only about 10 % were discarded at the shortest possible integration time of 60 ms and only about 2 % at the integration time of 120 ms. The NiCd battery was replaced with AA size nickel-metal hydride (NiMh) elements in 2 groups of 8 elements in series, connected in parallel (8S2P) configuration and a power supply unit was added for generating all the necessary supply voltages. An AHRS and a bidirectional reflectance factor (BRF) sensor were added. All this was fitted in a newly designed case.

The BRF sensor was based on a 256-band Si linear sensor array. The sensor was attached to a preamplifier DZA-S3901-4 by Tec5 AG. The FEE and controller were similar to those used for the MMS-1. With a wide-angle lens (DSL203 by Sunex Inc., FOV 140°), a transect along the flight path was projected through a band-pass filter onto the sensor. The cross-track FOV was limited to 10° with a slit that was glued to the window of the sensor. The along-track FOV was 140°, instantaneous field-of-view (iFOV) was 0.5° to 1° depending on the view nadir angle (VNA), being smaller near the nadir. The band-pass filter had 10-nm bandwidth. Either a red (660 nm) or NIR (850 nm) filter could be used but it was not possible to swap them during the flight.

AHRS is a device that provides the roll, pitch, and yaw information of the aircraft. This information became important with the inclusion of the BRF sensor. As long as the spectral measurements were done only in the nadir direction, the yaw information was irrelevant, the pitch angle did not change much, and the data collected at substantial roll angles when the aircraft was turning were discarded based on the GPS log. The AHRS was custom-designed and comprised 3 gyroscopic sensors, 3 accelerometers, 3 magnetometers, and a microcontroller. Unfortunately the quality of the sensors was insufficient and the recorded attitude angles unreliable. Gyroscopes measure angular velocities and integrating these over time gives us the attitude angles. Small bias errors cumulate over time and cause drift of the calculated angles. This drift is compensated with the accelerometers and magnetometers measuring the direction of the gravitational force and magnetic field of the Earth. These sensors do not have any long term drift effects, however, big short term noise is the problem for both of them. The data from all these sensors are fused together in a Kalman filter [20]. Helicopter can turn for several tens of seconds. Since the centrifugal force taints the accelerometer measurements, the contribution of the accelerometer data in the Kalman filtering process must be quite small. Hence, the gyroscopes must be of good quality and the long term drift has to be small. The gyroscopes used in the AHRS were not sufficiently stable and the drift of the calculated attitude angles unacceptably large.

2.3 UAVSpec3

UAVSpec3 is the current visible and near-infrared (VNIR) version of the series. It has been in use for the field measurements since 2008 [III, IV, VI]. The differences between the UAVSpec2 and UAVSpec3 are not very big. The NiMh AA size cells were replaced with a 4-cell lithium-ion polymer (LiPo) battery and the custom-made AHRS was superseded by MTi-G produced by Xsens Technologies B.V.

2.4 UAVSpec4SWIR

UAVSpec4SWIR is based on the miniature spectrometer module Near-Infrared Plane Grating Spectrometer 1.7 (NIR-PGS-1.7) by Carl Zeiss Jena GmbH. It has a plane grating with focusing and collimating lenses [21]. The sensor is a thermoelectrically cooled 256-band indium gallium arsenide (InGaAs) linear array. The fiber optic input is similar to the MMS-1 spectrometer module. Just as for the MMS-1, a preamplifier is integrated with the NIR-PGS-1.7. The sensor temperature is controlled by a PELTIER-tc controller manufactured by Tec5 AG. The PELTIER-tc is a linear temperature controller module with proportional-integrational (PI)-control which adjusts the current across the Peltier element to reach the sensor temperature equal to the preset setpoint temperature [22]. The sensor temperature is kept constant at +10 °C regardless of the ambient temperature. An external thermistor was glued next to the voltage reference integrated circuit on the preamplifier board to record the temperature changes during the measurement. A FEE-1M by Tec5 AG is used together with the NIR-PGS-1.7 spectrometer module. The custom-designed controller electronics, SBC, web camera, and GPS receiver are similar to those used in the UAVSpec3. Unlike the UAVSpec3, UAVSpec4SWIR does not have an AHRS and a BRF sensor.

3 CHARACTERISATION OF THE SPECTROMETERS

For acquiring reliable measurement results it is crucial to know the properties of the measuring instrument. Miniature spectrometer modules are rather primitive devices with very limited internal compensations for the impact of different environmental factors and spectrometer's own internal imperfections. In this study the dark signal temperature dependence and the instrument function of the spectrometer module were scrutinized and parameterized.

3.1 Dark signal temperature dependence

The output signal of a spectrometer contains two components — the dark signal and the target signal. The dark signal is an inherent property of a spectrometer. It is the output signal when the input aperture is closed. For extracting the target signal from the output signal, the dark signal must be subtracted.

The dark signal is not constant. It depends on the temperature, mainly due to the temperature dependence of a junction-based detector [23]. In paper II a dark signal temperature dependence correction method is described.

Dark signal temperature dependence was measured for the MMS-1, NIR-PGS-1.7, and NIR-PGS-2.2 miniature spectrometer modules. The measurements were done in a portable refrigerator at several different integration times. Since the refrigerator did not have a temperature controller, the measurements were done simultaneously with changing the temperature. The refrigerator's power supply was adjusted to limit the temperature change rate. The maximum temperature change rate was $0.7\text{ }^{\circ}\text{C min}^{-1}$, average was $0.15\text{ to }0.35\text{ }^{\circ}\text{C min}^{-1}$ for different spectrometers.

Heating the spectrometer module and its FEE one at a time revealed that only the temperature of the spectrometer module had significant effect on the dark signal. In Fig. 4 the measured temperatures of the spectrometer module and FEE are shown. At 14:44 the spectrometer module was heated for about two minutes. At 15:17 the FEE was heated for approximately two minutes. It is clear from Fig. 4 that the signal of band no. 150 follows the temperature of the spectrometer module and heating the FEE had virtually no effect on the dark signal. Therefore, only the spectrometer modules were placed in the refrigerator to minimize the emitted energy inside the refrigerator and maximize the attainable temperature range. For NIR-PGS-1.7 the Peltier current, setpoint voltage, and sensor temperature were measured with a Campbell 21X datalogger. The measurement setup is outlined in Fig. 1 in paper II. Only the temperatures recorded by the thermistor that is attached to the spectrometer module are considered in the correction algorithm.

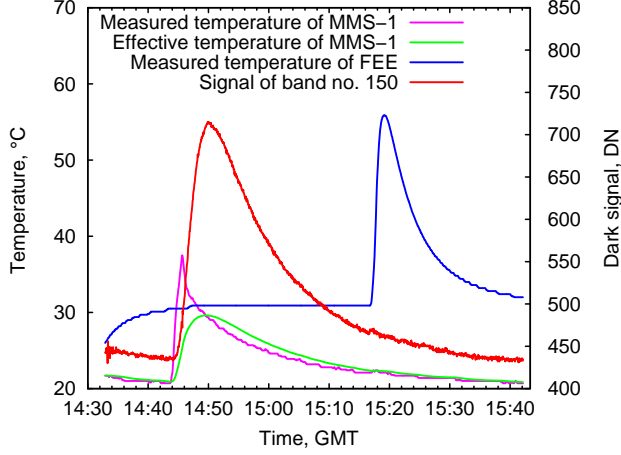


Figure 4. Dark signal during heating of the MMS-1 and FEE separately. The integration time was 3000 ms.

It is not possible to measure the actual temperature of the sensor of the MMS-1, because it is a sealed module and the sensor array is not accessible. Hence, the thermistor has to be attached to the spectrometer body. This, however, introduces a delay between the temperature change and the dark signal change. It is caused by the propagation time of the heat between the spectrometer body and the sensor array. Based on experimental results the following temperature model is proposed:

$$T_{e,i} = T_{e,i-1} + k(T_{i-1} - T_{e,i-1}), \quad (1)$$

where T is the measured temperature in °C, k is a parameter estimated in laboratory experiment, and $i = 2, 3, \dots, N$ is an index denoting the temperature measurements. It is assumed that $T_{e,1} = T_1$. To avoid dependence on the temperature sampling interval, the temperature measurements are resampled at 1 s interval. This model relates the measured outside temperature T to the effective temperature T_e of the sensor array that actually causes the dark signal change. The measured temperature, modelled effective temperature, and dark signal of the MMS-1 are plotted in Fig. 4.

The parameter k is related to the physical configuration of the spectrometer module and the thermistor. If the thermistor is removed for some reason, the parameter k must be re-estimated.

After calculation of the effective temperature for each spectrum measured in the refrigerator experiment, the dark signal temperature dependence correction parameters can be estimated. A second order polynomial function

$$f_{it}(T_e) = a_{it}T_e^2 + b_{it}T_e + c_{it} \quad (2)$$

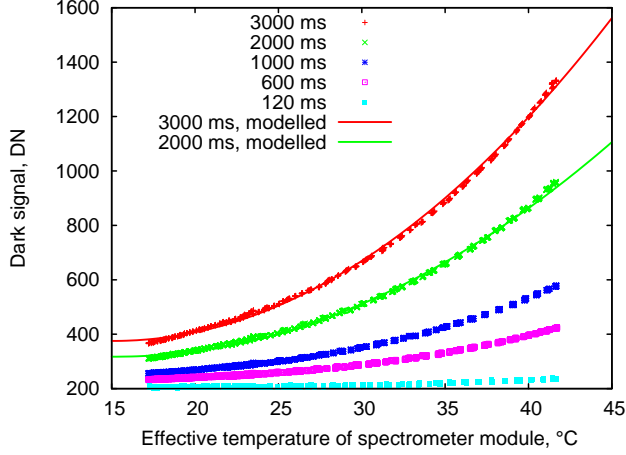


Figure 5. Dark signal temperature dependence of the band No. 150 of the MMS-1 at different integration times.

is fitted to every spectral band of the sensor array at every integration time used in the experiment. Here a_{it} , b_{it} , and c_{it} are the fitted parameters, t is the integration time, and i is the band number. Since the parameters a_{it} , b_{it} , and c_{it} are linearly related to the integration time [II Figs. 6 to 11] the Eq. (2) can be rewritten as

$$f_i(T_e, t) = a_i(t)T_e^2 + b_i(t)T_e + c_i(t), \quad (3)$$

where

$$a_i(t) = z_{1i}t + z_{2i}, \quad (4a)$$

$$b_i(t) = z_{3i}t + z_{4i}, \quad (4b)$$

$$c_i(t) = z_{5i}t + z_{6i}. \quad (4c)$$

If we know the fitted parameters z_{ji} , $j = 1, 2, \dots, 6$, then we can calculate the dark signal $f_i(T_e, t)$ for given effective sensor temperature, T_e , integration time t , and band number i . This means that not only can we model the dark signal at any temperature but the same model is applicable for any integration time. The dark signal temperature dependence of the MMS-1 spectrometer is plotted in Fig. 5. The modelled data $f_{150}(T_e, 2000 \text{ ms})$ and $f_{150}(T_e, 3000 \text{ ms})$ agree well with the measurements.

The dark signal of the NIR-PGS-1.7 at various temperatures and integration times can be seen in Fig. 4 in paper II. In case of the FEE-1M the dark signal offset is negative. The FEE-1M has a 16 bit ADC, the 16th bit is the sign bit. Since only a small range of negative values are in use, the effective resolution is roughly 15 bit.

Other parameters such as long term deterioration of electronic components can affect the dark signal of a spectrometer. To eliminate the error caused by these effects it is better not to rely only on the model but rather use it for estimating the dark signal $d_i(T_e, t)$ at any temperature T_e and integration time t based on the reference dark signal measurement d_{i,T_{0e},t_0}

$$d_i(T_e, t) = d_{i,T_{0e},t_0} + f_i(T_e, t) - f_i(T_{0e}, t_0), \quad (5)$$

where T_{0e} and t_0 are the effective sensor temperature and integration time, respectively, during the reference measurement.

Figure 4 in paper **II** shows that although the sensor of the NIR-PGS-1.7 is thermally stabilized, the dark signal is still related to the temperature. As the sensor of the NIR-PGS-1.7 has internal thermistor, it was possible to measure the relation between the dark signal and actual sensor temperature. The measurements confirmed that although the sensor temperature was not constant, the small change in the sensor temperature was not the cause of the dark signal change. Instead, most probable cause is that the preamplifier electronics is sensitive to temperature changes. So, it is important to keep in mind that thermally stabilized sensor does not necessarily eliminate the need for the dark signal temperature dependence correction. On the contrary, the NIR-PGS-2.2 by Carl Zeiss Jena GmbH with a thermoelectrically cooled extended InGaAs sensor [24] has about one order of a magnitude stronger dark signal temperature dependence compared to the MMS-1 with an uncooled Si sensor, as can be seen in Fig. 5 in paper **II**. One possible explanation to this is that although the sensor chip is cooled, it is still sensitive to thermal radiation from surrounding mechanics [25].

The correction algorithm is validated for the MMS-1 and NIR-PGS-1.7 on data collected during a 40 min flight with closed optical entrances in conditions similar to the actual field measurements. After the correction the remaining target signal should be zero since there was no radiation incident on the sensors. Figures 12 to 13 in paper **II** show that although the correction did not completely remove all the errors, it reduced the root mean square error (RMSE) by 36 % and 68 % for the MMS-1 and NIR-PGS-1.7, respectively.

3.2 Instrument function

Optical quality of miniature spectrometer modules is usually inferior to bigger spectrometers. Small size means less alternatives for reducing the stray light. The stray light in a spectrometer can be described as light that is not intended to be there. Instrument function (also known as slit-scattering function or apparatus function) describes the measured target signal of the spectrometer in case of monochromatic input. In ideal case the monochromatic light should hit only one

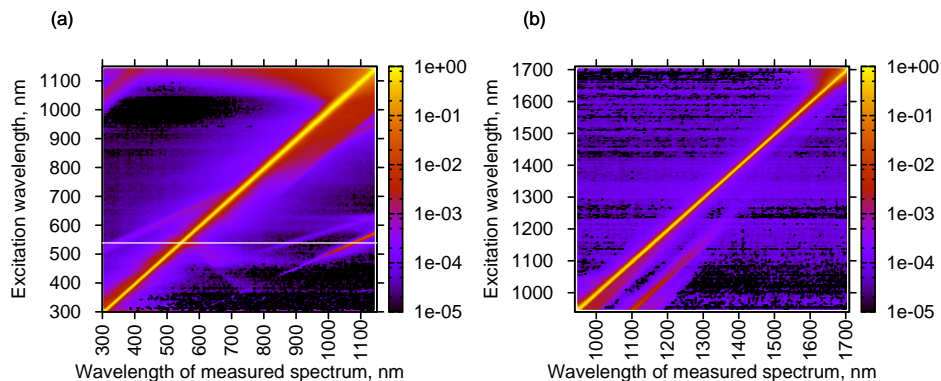


Figure 6. Measured instrument functions for the (a) MMS-1 and (b) NIR-PGS-1.7. The horizontal white line in (a) denotes the data plotted in Fig. 7.

pixel of the sensor, or a few neighboring pixels in case of oversampling, but the reality is rather different. Due to scattering on the grating, internal reflections, low quality order sorting filters and other imperfections of the spectrometer, some of the monochromatic light hits pixels corresponding to other wavelengths. The measured target signal of the spectrometer is the convolution of the actual optical input signal and the instrument function of the spectrometer.

The instrument functions of the MMS-1 and NIR-PGS-1.7 were measured with a double monochromator. A double prism monochromator ДМР-4 [26, 27] by Leningrad Optical Mechanical Amalgamation (Ленинградское оптико-механическое объединение) (LOMO) was used for the MMS-1, a double grating monochromator СДЛ-1 [26] also by LOMO was used for the NIR-PGS-1.7. The monochromator was scanned through the wavelength range of the spectrometer while the spectrometer continuously recorded the signal. Later, the measurements where the spectral line from the monochromator matched the spectrometer bands were automatically filtered out based on the criterion that the difference of the signals of neighboring two pixels was less than 20 % of the peak signal. This approach increases the full width at half maximum (FWHM) of the central peak less than half a pixel. All the measurements corresponding to the same pixel were averaged and normalized to the central peak.

The measured instrument functions for the MMS-1 and NIR-PGS-1.7 can be seen in Fig. 6. The horizontal white line in Fig. 6 (a) denotes the measurement at the monochromator setting of 538.8 nm. The relative response to this spectral line is plotted in Fig. 7.

In ideal case, the instrument functions in Fig. 6 should contain only the yellow

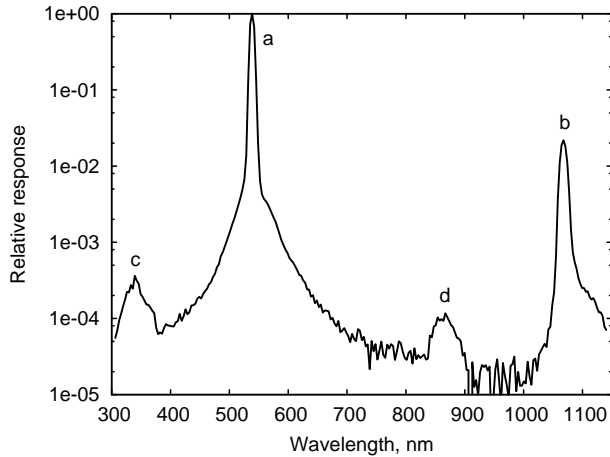


Figure 7. Relative response of the MMS-1 to the 538.8 nm spectral line. This is the instrument function for the pixel No. 71.

low 1:1 line on black background i.e. the signal should be recorded only at the pixels corresponding to the monochromator wavelength setting. All the rest of the features visible in the images are caused by imperfections of the instruments and noise in the very weak signal.

In Fig. 7 the instrument function for pixel No. 71 (538.8 nm) of the MMS-1 can be seen. It has four distinctive peaks. The peak marked with a is the main peak that corresponds to 538.8 nm which is the excitation wavelength. The instrument function is normalized to this peak. The wavelength scale of the spectrometer corresponds to the first order diffraction. The peak marked with b at 1067.7 nm is caused by the second order diffraction that passes through the order sorting filter which is directly coated on the sensor. The origins of the two other peaks marked with c and d can only be assumed. They are probably caused by interreflection between the sensor and the grating. According to the grating equation the second order maximum should coincide with the first order maximum of twice the wavelength, i.e. $2 * 538.8 \text{ nm} = 1077.6 \text{ nm}$. However, since the MMS-1 has a solid glass body, which has different refractive index for 538.8 nm and 1077.6 nm, the second order maximum of 538.8 nm and the first order maximum of 1077.6 nm do not coincide.

The second order diffraction peak is the most problematic feature of the instrument function of the MMS-1 spectrometer. Its amplitude is more than 2% of the main peak, but the sensitivity of the sensor in the visible spectral region is a lot higher than in the NIR spectral domain. In addition, the solar radiation, which is a commonly used illumination source in remote sensing applications, has the high-

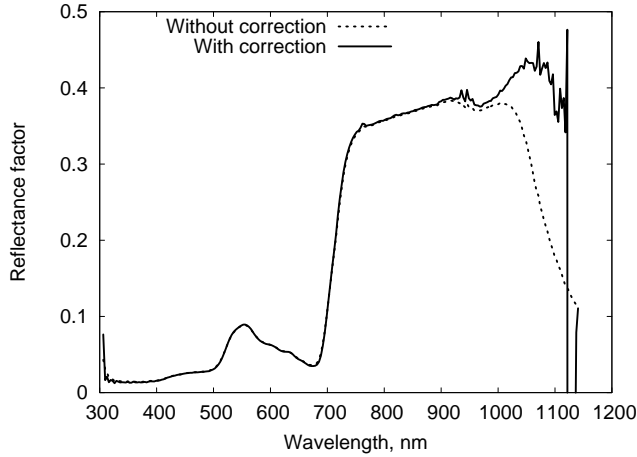


Figure 8. Reflectance of green vegetation with and without the stray light correction measured with the MMS-1 and calibrated gray Spectralon reflectance panel.

est radiant flux density in the visible spectral region. Therefore, when measuring a gray or white target like a Spectralon reflectance panel, at 1000 nm the ratio of the actual NIR signal and the second order diffraction signal from the visible spectral region is about 10:1. At 1050 nm, the respective ratio is 1:1 and at 1100 nm already 1:10 since the sensitivity of the sensor in the NIR spectral domain decreases strongly with increasing wavelength.

In Fig. 8 the reflectance of green vegetation is plotted. It is calculated as a ratio of the target and reference panel measurements (see Eq. (6)). The reflectance spectra of these two objects are very different. For the reference panel it is roughly constant over the entire measured spectral range whereas for the green vegetation the reflectance values in the visible spectral region are much lower than in the NIR part of the spectrum. This means that the second order diffraction signal in the target measurements is weaker than in the reference measurements. The measured signal and corrected signal of the green vegetation and reference panel can be seen in Fig. 9. The integral of the signals is normalized to one. It is clear from the figure that the influence of the correction is stronger for the signal of the reference panel. So, without the stray light correction the reflectance factor calculated with Eq. (6) decreases rapidly with increasing wavelength in the spectral region where the second order diffraction signal becomes significant.

The output signal of the spectrometer is the convolution of the input optical signal and the instrument function. If the instrument function is known, then the original signal can be restored by deconvolution [28]. The effect of correction can be seen in Fig. 8. By applying the correction to the measured spectra, reliable

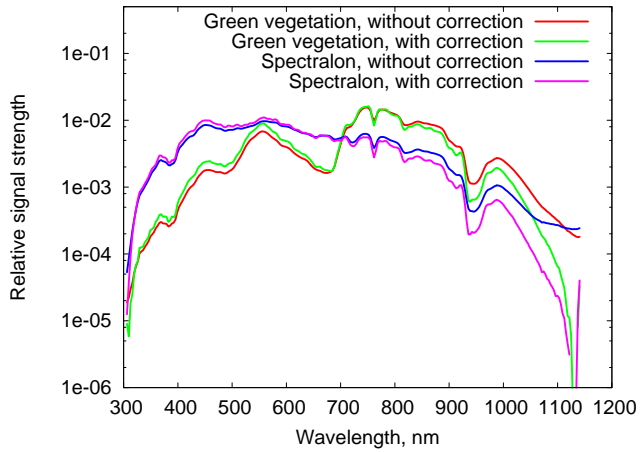


Figure 9. Signals of green vegetation and the reference panel with and without the stray light correction. The signals were measured with the MMS-1. The integral of the signals is normalized to one.

spectral range can be extended by 100 nm in case of the MMS-1. NIR-PGS-1.7 does not have the problems caused by the second order diffraction since the higher order diffraction peaks are outside of the spectral range of the spectrometer. Therefore, the effect of the correction is not so strong.

4 FIELD MEASUREMENTS

The field measurements were carried out at the test site located in Järvelja, Estonia, 27.3 °E, 58.3 °N. The test site is situated in the Järvelja Training and Experimental Forestry District of the Estonian University of Life Sciences. The area is covered with hemiboreal forests which are regularly managed. The last forest inventory data was collected in 2001. The same area has served as a test site for the POLDER mission [29] and VALERI project [30]. Two 100 m × 100 m plots in this area were used for defining the test cases in the fourth phase of the RAdiation transfer Model Intercomparison (RAMI) [31]. More information of the site is provided by Kuusk et al. [32], the detailed description of the RAMI plots is presented by Kuusk et al. [33].

In 2006 and 2007 the TOC spectral reflectance factor of hemiboreal forests was measured with the UAVSpec and UAVSpec2, respectively. Both of the instruments were mounted to the chassis of a Robinson R22 helicopter so that they were looking in the nadir direction during straight flight at constant speed. Average flight altitude was approximately 100 m agl in 2006 and 80 m agl in 2007. Considering the 2° FOV, 120 ms integration time, and 60 km h⁻¹ flight speed, the diameter of the footprint of the FOV on the ground was about 3 m and 2.5 m in 2006 and 2007, respectively, and during a single measurement the helicopter moved forward 2 m. The flight trajectory was selected so that it covered large and homogeneous stands of different species, age, and site type.

Since 2008 the UAVSpec3 and since 2009 the UAVSpec4SWIR have been used every summer for measuring the TOC spectral reflectance of forests over the Järvelja test area. An average measurement campaign comprised approximately one hour flight over the forests during which more than 20 000 spectra over more than 400 stands were acquired. The setup was similar to previous years except the integration time of the UAVSpec3 measurements has been increased to 150 ms since 2009. For the UAVSpec4SWIR, the integration time during the TOC reflectance measurements has been 100 ms.

In 2007 and 2008 the spectral directional reflectance factor of the understory of the RAMI plots was measured with the UAVSpec2 and UAVSpec3, respectively. A 8° FOV restrictor and a 5 m extension fiber by Analytical Spectral Devices Inc. (ASD) were used. The FOV restrictor was attached to a self-leveling mount which eliminated any systematic error in the VNA caused by holding the spectrometer in hand while walking around in the forest. The measurements were carried out at 9 locations in each of the stands while walking slowly along a nearly circular transect of 5 m radius [33]. The measurements were made at the height of about 1 m. Illumination was measured at every transect with a RCR by ASD right after the reflectance measurement. The RCR was attached to the same self-leveling mount as the downward-looking lens and the extension fiber was inter-

changed between them. Similar measurements were carried out over a Spectralon reflectance panel at a nearby clearing to calibrate the instruments and link the measurements to the radiometric scale. The measurements were carried out in cloudless weather conditions to minimize the errors caused by changing illumination.

4.1 Calculation of reflectance factor

First, the dark signal is calculated separately for every spectral band of every measurement according to the dark signal temperature dependence correction algorithm described in paper **II**. The corrected dark signal is subtracted from the output signal of the spectrometer. Then, by deconvolution the original optical signal is extracted from the measured target signal [28]. Next, the recorded digital numbers (DNs) n_λ are converted to target reflectance values ρ_λ with the help of a Spectralon reflectance panel having a calibrated reflectance factor r_λ and a reference spectrometer equipped with an RCR measuring the incident spectral flux density Q_λ

$$\rho_\lambda(t) = \frac{q_\lambda(t_0) n_\lambda(t)}{n_\lambda(t_0) q_\lambda(t)} r_\lambda. \quad (6)$$

Here, q_λ is the signal recorded by the reference spectrometer, t and t_0 are the times of the target and reference panel measurements, respectively. The use of a reference spectrometer accounts for the diurnal change of illumination, but also allows to estimate the atmospheric conditions during the measurements. The atmospheric correction of the measured data is not necessary because when flying at the altitude of 80 m agl, less than 1 % of the atmosphere by mass is between the sensor and the target. After calculation of the reflectance factors, the GPS data is interpolated to every single spectral measurement which allows to use the data in a geographic information system (GIS). Finally, the status of the targets and the accuracy of geolocation can be visually verified from the web camera images. The footprint of the FOV of the spectrometer is marked with a red circle in each image (see Fig. 10).

The data processing flowchart is outlined in Fig. 11. FieldSpec Pro VNIR by Analytical Spectral Devices Inc. and SVC HR-1024 by Spectra Vista Corporation have been used as ground based reference spectrometers. Their metrological quality is guaranteed by the manufacturers and post-processing of the measurement data is not necessary.



Figure 10. A sample UAVSpec3 web camera image. The red circle marks the footprint of the FOV of the spectrometer. Between the two red lines is the footprint of the FOV of the BRF sensor (extends over the image borders).

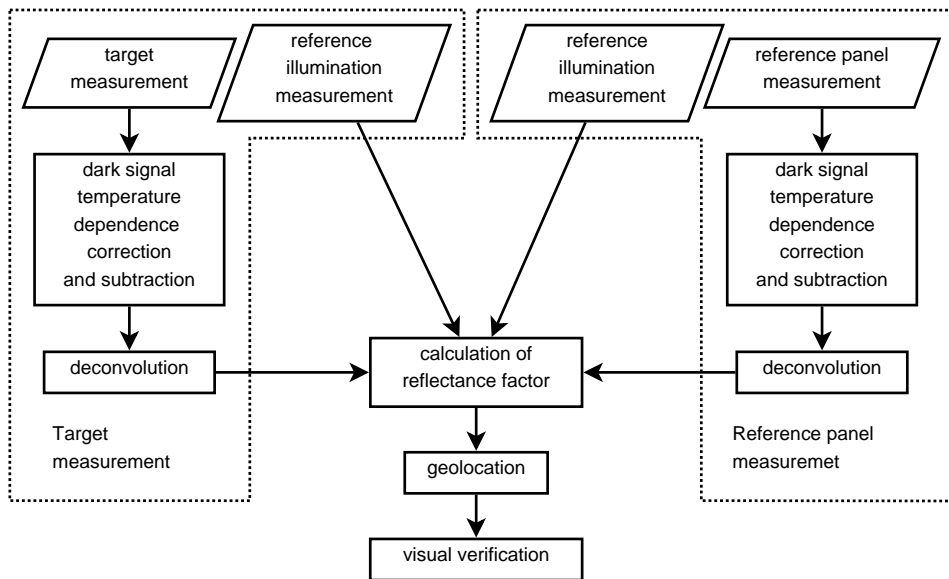


Figure 11. Data processing flowchart of the field measurements of the TOC spectral reflectances.

5 RESULTS AND DISCUSSION

5.1 A dataset for the validation of reflectance models

Vegetation radiative transfer models need many different input parameters. The accuracy of the model simulations obviously depends on the quality of the used algorithm, but also on the available input data. The first rule of modelling: garbage in, garbage out. If the available input data is not accurate, sufficient, or compatible, even the best model can not give correct results. For validating a model, it is essential to have the best possible set of input data. Paper **III** describes a dataset for the validation of vegetation reflectance models.

The dataset is based on three 100 m × 100 m stands in the Järvelja region. These are a 124-year-old pine (*Pinus sylvestris*) stand, a 49-year-old spruce (*Picea abies*) stand, and a 59-year old birch (*Betula pendula*) stand. These stands were selected based on a query from forestry database and on-site visual inspection. The main criteria for the selection were preferably pure, middle-aged or older homogeneous stands big enough for establishing the sample plots and measuring the reflectance from satellite images.

Stand structure measurements were carried out in 2007. In each stand all the trees with the diameter at breast height (DBH) greater than 4 cm were tallied and their exact locations relative to the stand zero-point were measured with a total station. Tree height, height to live crown base, and two perpendicular crown diameters were measured for the sample trees in each plot. Allometric models were used for estimating these parameters for the rest of the trees. Effective leaf area index (LAI) was measured with an LAI-2000 plant canopy analyzer in each plot on the regular grid of 9 points, the grid step being 30 m. Upward-looking hemispherical color images were taken at the same points. Gap fractions were estimated from these images. A Cajanus tube was used for measuring canopy closure and crown closure. In the birch stand the LAI was measured again in winter to estimate the share of stems and branches in forming the canopy cover.

Reflectance spectra of understorey vegetation was measured at the end of July in 2007 and 2008 with the UAVSpec2 and UAVSpec3, respectively. The measurements were done at circular transects around the LAI measurement points. Directional-hemispherical reflectance and transmittance of birch, alder, and aspen leaves in the birch stand, and reflectance of a bundle of needles of a live shoot in the pine stand were measured in 2007 and 2008 using the UAVSpec2 and FieldSpec Pro VNIR, respectively, equipped with an integrating sphere. Reflectance spectra of stem and branch bark were measured similar to the leaves. Stem bark measurements for some species had been carried out previously with a GER-2600 spectrometer using natural illumination [34].

TOC spectral reflectance of the stands were measured in 2007 and 2008 with

the UAVSpec2 and UAVSpec3, respectively, from an airborne platform. The same information for 2005 was extracted from a recalibrated Compact High Resolution Imaging Spectrometer (CHRIS) image [IV].

On 30 July 2009, airborne laser scanning of the stands was carried out from the altitude of 500 m agl. The total point density was about 20 points per m².

All the details of measurements, instruments in use, data processing and access to the data are described by Kuusk et al. [33].

5.2 Vicarious calibration of satellite sensors

Satellite sensors go through exhaustive pre-launch calibration procedures. The preflight calibrations, however, are subject to change during the launch and in the space environment. During service the importance of the on-orbit calibrations increase, but the onboard calibration facilities may also degrade over time [35]. Some satellites do not have any onboard calibration facilities at all [36, 37] or they are used only for relative calibration [38]. Vicarious calibration methods can be utilized for absolute calibration of the operational satellite sensors. In this case, natural Earth scenes are used for calibrating the sensor [39]. In paper IV revised calibration coefficients for the CHRIS onboard the Project for On Board Autonomy (PROBA) satellite are proposed based on airborne reflectance measurements of mature hemiboreal forests.

Three CHRIS Mode 3 images were acquired over the Järvelja test site on 10 July 2005. The acquisition details are listed in Table 1 in paper IV and the Mode 3 spectral bands in Table 3 in paper IV. The airborne measurements were carried out on 26 July 2006 with the UAVSpec. The aerosol optical thickness (AOT) was very low during both, the PROBA overpass and the airborne measurements [IV Fig. 1]. This means that the atmospheric correction of the imagery is less sensitive to atmosphere parameters. Vicarious calibration of satellite sensors rely on the accuracy of the atmospheric correction of the satellite data and the quality of the reference measurements.

Processing of the CHRIS images comprised multiple steps. First, the images were destriped. Different transfer functions of the sensor elements cause stripes in the image [40]. It was assumed that the stripes were caused by the differences of analogue offsets of the recorded signals. The destriping function was found for every image as the difference between the column mean values and the smoothed column mean values using a 9-point Hamming window. The mean value of the three destriping functions for every band was used for all the three respective spectral images.

Next, a two-step atmospheric correction of the image was made. A look-up table which linked the TOA radiances to TOC reflectances was created with the atmospheric radiative transfer package 6S using the method proposed by Kuusk

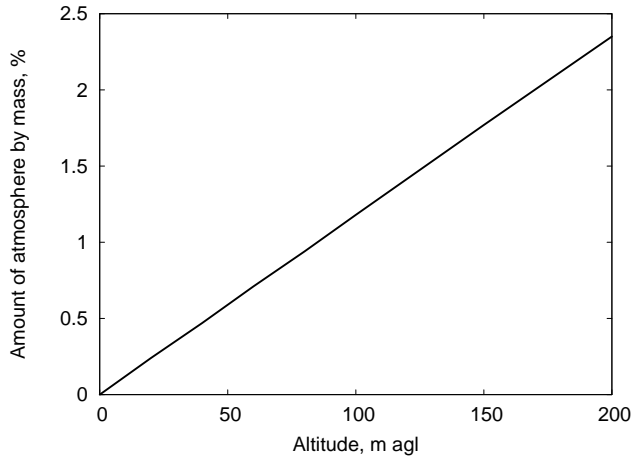


Figure 12. Amount of the atmosphere by mass between the sensor and the ground depending on the flight altitude.

[41]. In the second step, the adjacency effect was removed by two-dimensional deconvolution. The atmosphere acts as a low pass filter and the image recorded by the satellite sensor is the convolution of the TOC radiance pattern and the point spread function (PSF) of the system atmosphere-sensor [42]. Degraded images can be restored by Wiener filtering in the Fourier space. The Wiener filter includes the power spectral density of the noise and the Fourier transform of the PSF [43].

The noise spectrum was assumed to be exponentially increasing with spatial frequency. Its magnitude was estimated using the signal-to-noise ratio from the CHRIS documentation and the mean reflectance of every spectral image.

The PSF of the atmosphere was estimated by Liang [44] in numerical simulations. However, using the suggested parameters resulted in overestimating the adjacency effect and negative reflectance values of a small lake in the CHRIS scene. Since the reflectance of water can be very low, but definitely positive, the parameters were rescaled to provide reasonable reflectance values for the water bodies.

The adjacency effect is most influential for areas with very contrasting neighbours, e.g. a mature forest and a gravel road. For some stands in some spectral bands the effect of adjacency correction may reach even 15 to 20% of the stand reflectance.

The accuracy of the airborne measurements is determined by the gain and offset errors of the spectrometers and the errors in the reference reflectance [IV Eq. (11)]. The Spectralon reflectance panel which has very uniform and stable reflectance value was used as the reference. The airborne measurement results

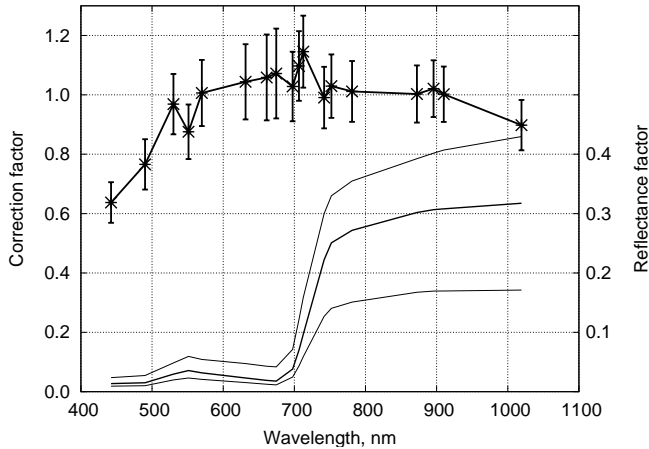


Figure 13. Correction factors for the CHRIS calibration coefficients (the upper curve) and the mean stand reflectance and the range of stand reflectances involved in the comparison (the three lower curves).

were corrected for the dark signal temperature dependence and errors caused by the stray light. When measuring a 20 m high forest from the altitude of 100 m agl, less than 1 % of the atmosphere by mass is between the sensor and the target (Fig. 12). Therefore, atmospheric correction of the airborne measurements was deemed unnecessary.

A set of large, mature, and homogeneous stands was selected representing all the dominating species at the test site. Spectral bands of the UAVSpec were combined to match the bands of the CHRIS spectrometer. Altogether 1302 UAVSpec spectra over 520 CHRIS pixels over 63 stands were compared. The TOC reflectances calculated from the CHRIS images were reduced to the nadir direction with the FRT forest reflectance model [16]. Each stand was handled separately using the species-specific stand structure parameters from the forestry database.

The ratio of the mean stand reflectance from the airborne measurements to the nadir adjusted CHRIS TOC reflectances was calculated separately for every stand. The correction factors for the CHRIS calibration coefficients were calculated as the mean of these ratios over all the 63 stands. The correction factors can be seen in Fig. 13 and are listed in Table 3 in paper IV.

Bright uniform targets should be used for vicarious calibration [45]. Unfortunately there are no such targets in the Järvelja area. Since PROBA is a small satellite, it has limited amount of resources for maintaining stable temperature of the scientific instruments [46]. Therefore, frequent calibrations are advisable, in ideal case for every scene since the temperature of the satellite depends on the time passed since the eclipse. CHRIS has also very limited acquisition resources

— only 2 to 3 sites per day. This hinders the feasibility of making numerous calibration acquisitions over suitable areas.

The main shortcoming of the calibration described in paper **IV** was the one year difference in the satellite and airborne acquisitions. The CHRIS image was from 2005 but the UAVSpec measurements were carried out in 2006. In paper **V** it was shown that short term variations in the reflectance factor of mature forests can be rather significant. Analyzing the mean values of Moderate Resolution Imaging Spectroradiometer (MODIS) nadir bidirectional reflectance distribution function (BRDF)-adjusted reflectances over $7 \text{ km} \times 7 \text{ km}$ area centered at the CHRIS scene revealed that year 2005 was more similar to 2006 than to 2007 in terms of the forest reflectance. Hence, the correction factors provided in paper **IV** may be slightly over-estimated but the difference is smaller than the differences described in paper **V**.

Although the credibility of the provided correction factors is not very high, the method described in paper **IV** remains valid and can be used in the future for simultaneous measurements from the satellite and airborne platforms.

5.3 Comparison of measurements at different years

Previous studies have shown that in long term the reflectance of mature forests is relatively stable [17, 47, 48]. Several stands of the test site were measured both, in 2006 and 2007. This allowed to verify if this is also the case in short term. In paper **V** the reflectance measurements of the same stands at two consecutive years is compared. The years 2006 and 2007 differed significantly in the amount of rainfall. 2006 was very dry whereas 2007 was average year for the region (see Fig. 14). The measurements were not done at the same dates of the year but the difference in degree days (DDs), which better describes the phenology stage of the vegetation [49], was only 49 DD.

The atmospheric conditions during the measurements were rather different [**V** Table 2]. 26 July 2006 was very clear whereas 8 August 2007 was hazy. The Sun elevation also differed approximately 2° . These differences were taken into account and the reflectance data of 2007 were normalized with the FRT forest reflectance model [16] to match the measurements of 2006.

A very careful selection of stands was made to minimize the errors caused by the inhomogeneity of the stands and differences in the flight paths at different years. Eight silver birch (*Betula pendula*), four black alder (*Alnus glutinosa*), three Norway spruce (*Picea abies*), and two Scots pine (*Pinus sylvestris*) stands were selected for the analysis [**V** Table 3]. In addition to the mature stands, an alder-birch swamp with grass and no trees was included in the study set. To even further ensure the conformance of the measurements, a 1.1 km transect was selected where the two flight lines almost coincided. From this point on this transect

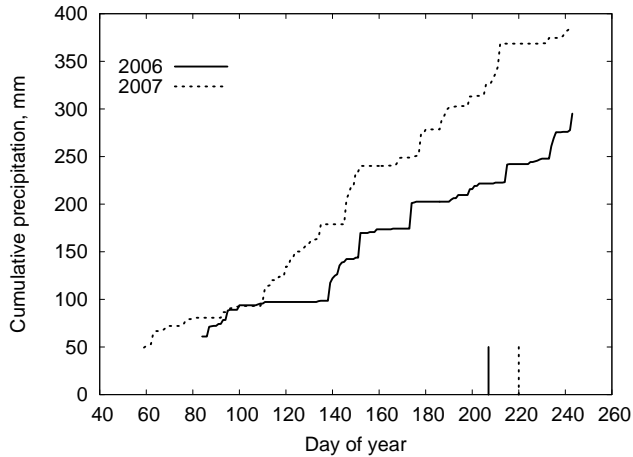


Figure 14. Cumulative precipitation at the test site in 2006 and 2007. The vertical bars denote the time of the reflectance measurements

will be referred to as the 'long transect'.

First, the mean of single measurements of each stand was calculated. Next, the ratio of the mean reflectances in 2006 and 2007 was calculated for each stand. Finally, the ratios were averaged over the stands of the same species. Each line in Fig. 15 represents the average ratio of the stand mean reflectances in 2006 and 2007. The results for the long transect and swamp are missing from this figure due to lack of the ground truth measurements needed for the FRT model. Without considering the illumination differences the average ratio of mean reflectances for these two cases can be seen in Fig. 11 in paper V.

The results in Fig. 15 show that the reflectances measured in the dry year (2006) were higher throughout the whole VNIR spectral region of the MMS-1 spectrometer module. In the visible spectral domain the broadleaved and coniferous forests are distinctly grouped in the figure. The spruce stands have the highest difference in reflectances reaching even 30 % in the blue bands. The difference is smallest for the broadleaved forests in the red chlorophyll absorption band. The change is 10 to 20 % for all the species in the NIR spectral region. While there remains some doubt about the accuracy of the results in the visible region due to low reflectances and possible errors in determining the dark signal level, there are no such concerns in the NIR spectral domain. The error bars in Fig. 15 mark the standard deviation of the stand mean ratios. The relatively large standard deviations are caused by low number of stands from each species.

Based on the available data it is not possible to determine which scene components cause the observed differences in the reflectance of mature forests. Due

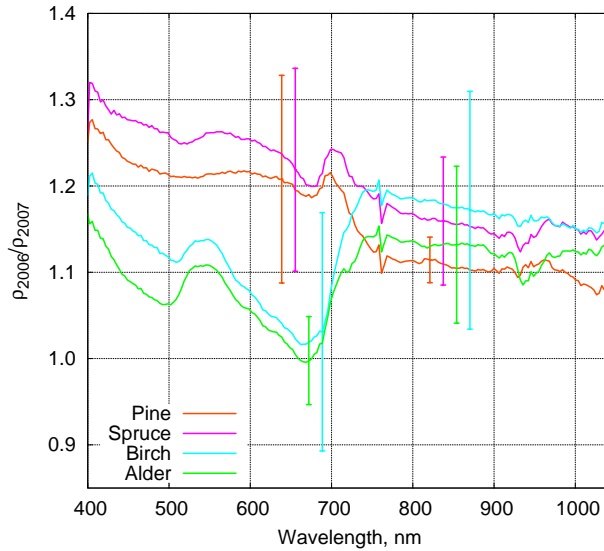


Figure 15. Average ratio of the stand mean reflectances in 2006 and 2007 while taking into account the Sun angles and atmosphere parameters.

to smaller roots the understorey vegetation is more influenced by the moisture conditions. Broadleaved stands had higher canopy closure than coniferous stands [V Table 3], so less undergrowth was visible. However, there is no reason to exclude the possibility of change in the optical properties of the leaves and needles of the trees. Nevertheless, the study showed that short term variations in reflectances of mature forests can be unexpectedly significant. If the forests are used as the dark objects in the atmospheric correction of satellite images [44] then the subpixel structure of the pixel reflectance is irrelevant and overall changes of the stand reflectance caused by the weather conditions should be taken into account.

5.4 Comparison of simulations and measurements

The pine and birch stands from the dataset described in paper III were used for defining the test cases for the fourth phase of the RAMI exercise [31]. The official results of RAMI are not yet disclosed. In paper VI the measured TOC spectral reflectance data of the three stands described in paper III and by Kuusk et al. [33] are compared to the simulations with the FRT model [16].

Although in the RAMI stands as many different parameters as possible were measured [33], some of the parameters needed for the FRT were still missing. The Biochemical properties of leaves and needles were not measured. Instead, the leaf optical model PROSPECT [50] was fitted to the measured spectra of the leaf

and needle hemispherical reflectance and transmittance factors. The PROSPECT model serves as a submodel for the FRT. It was not possible to measure the optical properties of a single needle of coniferous species. The reflectance of a shoot was measured and the reflectance factor of a single needle was calculated inverting the layer model by Gausman et al. [51]. Transmittance of a needle in 18 spectral bands was obtained from the RAMI website [31]. Structural and optical properties of the ground vegetation were not measured. A two-layer Canopy Reflectance Model (ACRM) [52], which serves as a submodel for the FRT was fitted to the measured directional reflectance spectra of the understorey vegetation.

The measured TOC spectral directional reflectance factors [VI Figs. 11 to 13, marked as UAVSpec] are compared to the model simulations with different input parameters. The curves marked as FRT-1 are the results when using all the available input data. FRT-2 denotes the simulations with adjusted input parameters to get better fit to the measured data. The RAMI IV simulations had some restrictions to the models and input parameters [31] and the simulations with these parameters are marked as FRT-3. There is no FRT-3 line for the spruce stand as it was not involved in the RAMI exercise. Out of the three stands, the birch stand is closest to a homogeneous canopy, therefore, a simulation was made with the ACRM model.

There are several causes to the discrepancy between the simulated and measured reflectances plotted in Figs. 11 to 13 in paper VI. Some of them can be attributed to imprecise input data. Instead of measuring the reflectance of a single conifer needle, a bunch of needles were used and the reflectance of a single needle was obtained from a model, which does not take into account various properties of the target and aspects of the measurement setup. Transmittance of a needle was not measured at all but obtained from the RAMI dataset. Reflectance values of adaxial and abaxial leaves may differ nearly two times in the visible spectral region. Leaf side is not explicitly included in the FRT model and an average value must be used. When looking in the nadir direction mainly the darker adaxial side is visible, however, in case of multiple scattering both sides contribute. Leaf orientations were not measured and spherical orientation was assumed for the birch stand. The area of leaves and branches can only be estimated by indirect measurements and the magnitude of errors is difficult to assess. The measured tree positions and crown radii in the plot do not give the canopy cover since the tree crowns are not symmetrical and centered over the trunk. Therefore, the calculated probability of seeing the understorey is not solid.

In the pine stand the simulated reflectance values are systematically higher than the measured values [VI Fig. 11]. By adjusting input parameters the measured reflectance curve can be reproduced by simulation with great precision. However, the necessary adjustments of the input parameters do not have ratio-

nal explanations in real life. It seems that the model underestimates the amount of shadows in the scene to some extent.

In the spruce stand the modelled reflectance values are rather close to the measured ones and only small adjustments of the input parameters are necessary for getting a good agreement between them. One possible explanation to this is that the spruce stand includes nearly 20% of deciduous trees and the mixture of coniferous and deciduous trees compensate some modelling problems of the corresponding pure stands.

The interpretation of the simulation results of the birch stand is most complex. The modelled reflectance in the green bands is higher than the measured one but the situation is opposite in the NIR bands. In addition, the slope of the spectral curve in the NIR spectral region can not be reproduced with the model. Adjusting the input parameters brings the simulated values closer to the measured ones but good agreement in the NIR spectral domain can not be attained. There is no simple explanation to the discrepancies between the model and the measurements. The homogeneous two-layer model systematically overestimates the reflectance values which is anticipated because it does not consider the shoot level and crown level clumping effects.

The share of multiple scattering in the FRT simulations is in rather good agreement with the estimated ones. Differences can be explained by inadequate estimation of the single scattering albedo in the calculations used for separating the single and multiple scattering components in the stand reflectance. In the birch stand only the leaf single scattering albedo was taken into account whereas the non-green elements also contribute. In coniferous stands the reflectance and transmittance of a single needle could not be directly measured, so the single scattering albedo may be incorrect. In addition, the share of single scattering may be overestimated.

The spectral invariant p — the photon recollision probability can be estimated from Eq. (7) in paper VI. In an x-y-plot $\rho(\Omega, \lambda)/\omega(\lambda)$ versus $\rho(\Omega, \lambda)$, the points should lie on a straight line where p is the slope and $e(\Omega) q_0$ is the intercept of the regression line (ρ – directional reflectance factor, Ω – view direction, λ – wavelength, ω – single scattering albedo, $e(\Omega)$ – photon escape probability, q_0 – interceptance of the canopy). Figure 15 in paper VI shows the modelled and measured results. The difference from the theory has several reasons. The single scattering albedo should be a weighted average of the single scattering albedos of different species and of branch and trunk bark. In addition, the significant violation of linearity at low reflectance values for coniferous species can be attributed to the division of two small values with possibly large errors and the small number of recollisions. Several assumptions that are not fulfilled were made for Eq. (7) in paper VI. Another simulation was made with those assumptions satisfied. As a

result a perfectly linear relation was obtained [VI Fig. 16, marked as FRT-2]. This fact confirms that FRT is able to adequately model the basic radiative transfer features mostly related to the description of multiple scattering.

The comparison revealed several problems of the FRT model. Since FRT positioned well compared to other models in the third phase of RAMI [53], similar problems are expected for the rest of the models as well. Estimation of (visible) shade probabilities in the canopy and on the ground surface should be reviewed. Difficulties in simulating the NIR reflectances suggest problems in reckoning with multiple scattering. As always, one of the severest problems is the adequate characterization of various parameters of the actual forest stands.

SUMMARY

Vegetation is an important part of the ecosystem and significant driving factor of the climate system. Due to this, studying and monitoring the vegetation has been one of the key targets of remote sensing. Evolution of the Earth observation satellites in the second half of the 20th century has significantly expanded the opportunities for remote sensing. A satellite can cover large area at a time and if the weather conditions allow it is easy to repeat the measurement. For extracting some meaningful information from the measured data it is necessary to understand how the measured signal is formed and what affects it. Vegetation radiative transfer models embrace this knowledge base. They can simulate the absorption and scattering of the solar radiation depending on the properties of the canopy and understorey.

Ground truth data is necessary for developing the models and validating remote sensing methods. Simulated data can be compared to the actual measurement results and in case of discrepancies the model should be altered. It is quite obvious that the accuracy of the measured data is crucial for this task. Satellite sensors record the signal that has passed through the layer of atmosphere between the target and the sensor. This degrades the measured signal. Therefore, the best results can be achieved by measuring the solar radiation scattered by forests from as low altitude as possible. This guarantees that the effect of the layer of atmosphere between the sensor and the target is insignificant. Top-of-canopy (TOC) measurements are also needed for validating the quality of atmospheric correction and radiometric calibration of satellite data.

There have been numerous airborne measurements of forest spectral reflectance but they have all been made from the altitude higher than 500 m above ground level. Usually the forest inventory data is insufficient or missing at all. Measurements at Järvselja are supported by the forest inventory data which are updated every 10 years. It is also difficult to synchronize the measurement campaigns with expensive instruments and large aircrafts to the satellite acquisitions. TOC measurements have been done from stationary masts, but this has very limited spatial coverage. The aim of this study was to design and build suitable equipment for measuring the TOC spectral directional reflectance of forests and to carry out actual measurements.

The UAVSpec-series spectrometer systems have been designed and built in the course of this study [I]. Since 2006 the TOC spectral directional reflectance of forest stands has been measured every summer in the Järvselja Training and Experimental Forestry District of the Estonian University of Life Sciences. The reflectance spectra of the understorey vegetation were measured in three stands in 2007 and 2008.

One of the objectives has always been the possibility to use an unmanned

aerial vehicle (UAV) as a carrier. Hence, the instruments were designed fully autonomous, and sufficiently small and light. Size and weight limitations dictate the selection of components. Miniature spectrometer modules by Carl Zeiss Jena GmbH have been used for the UAVSpec-series spectrometer systems. Unfortunately there is a tradeoff between the size and optical quality. In addition, the modules are not end-user products and characterizing the metrologically important parameters is the obligation of the designer. Based on the laboratory measurements, the dark signal temperature dependence was parameterized [III]. The stray light and spectral aliasing properties of the modules were studied. In order to guarantee the metrological quality of spectroscopic measurements, the parameters determined in the lab are taken into account in the data processing workflow.

Vegetation radiative transfer models need many input parameters which are not measured during the ordinary forest inventories, An exhaustive dataset was compiled for three stands in Järvselja [III]. These were 1 ha pine, spruce, and birch stands. The pine and birch stands were used for defining the test cases in the fourth phase of the international RAdiation transfer Model Intercomparison (RAMI) exercise. It was the first time in the 10-year history of RAMI when real stands were used as the test objects. The UAVSpec-series instruments were key tools in creating this database.

An acquisition over the Järvselja test site was made on 10 July 2005 by the CHRIS spectrometer onboard the European Space Agency's experimental satellite PROBA. Unfortunately the first UAVSpec-series instrument was not ready until 2006. Therefore, the time difference between the satellite and airborne measurements was one year but both were done at the same phase of the phenology cycle. Based on these results a detailed workflow description was proposed for processing satellite imagery and calibrating satellite sensors [IV]. Although the proposed correction factors for the CHRIS calibration coefficients may not be very reliable due to the aforementioned one year time difference, the same workflow can be used in the future for processing simultaneous measurements.

Large differences in the amount of precipitation in 2006 and 2007 provided an opportunity to study how the spectral reflectance of mature forests depend on the amount of precipitation. A selection was made from the data gathered during these two years based on the criteria that the measured stands were sufficiently large and homogeneous, and measured in both years. The comparison revealed that although the long-term reflectance of mature forests has been considered stable, the short-term variations can be rather significant exceeding even 20 % in some spectral regions [V]. This must be kept in mind when using the dark object method for the atmospheric correction of satellite images.

The forest reflectance model FRT developed at the Tartu Observatory was used for modelling the reflectance of the three stands described in the database.

The simulations were compared to the actual measurements [VI]. The comparison revealed some problems with the model. It seems to misjudge the shadowing in the canopy and on the ground. Problems with modelling the reflectance spectra in the NIR spectral region indicate possible problems in handling multiple scattering. Once again the basic modelling principle that the accuracy of the simulated data is greatly influenced by the accuracy of the input data was concluded.

REFERENCES

- [1] F. C. Billingsley, “Remote sensing for monitoring vegetation : an emphasis on satellites”, in *The role of terrestrial vegetation in the global carbon cycle : measurement by remote sensing*, G. M. Woodwell, Ed., Published on behalf of the Scientific Committee on Problems of the Environment (SCOPE) of the International Council of Scientific Unions (ICSU) by John Wiley & Sons Ltd, Chichester [West Sussex], 1984, pp. 161–180.
- [2] A. Marçal, Ed., *Global Developments in Environmental Earth Observation from Space*. Millpress, Rotterdam, Netherlands, 2006.
- [3] M. A. Wulder and S. E. Franklin, Eds., *Remote Sensing of Forest Environments : Concepts and Case Studies*. Kluwer Academic Publishers, Dordrecht, Netherlands, 2003.
- [4] B. Hapke, “A theoretical photometric function for the lunar surface”, *Journal of Geophysical Research*, vol. 68, pp. 4571–4586, 1963.
- [5] P. Oetking, “Photometric studies of diffusely reflecting surfaces with applications to the brightness of the moon”, *Journal of Geophysical Research*, vol. 71, no. 10, pp. 2505–2513, 1963.
- [6] K. Kriebel, *Reflection properties of vegetated surfaces: Tables of measured spectral biconical reflectance factors*. Wissenschaftliche Mitteilungen des Meteorologischen Instituts der Universität München, 1977, p. 82.
- [7] A. Kuusk, J. Anton, T. Nilson, U. Peterson, K. Ross, J. Ross, and A. Savihhin, “Reflection indicatrices of vegetation covers”, *Soviet Journal of Remote Sensing*, vol. 4, no. 5, pp. 802–813, 1985.
- [8] M. V. Schönemark, B. Geiger, and H. P. Röser, *Reflection properties of vegetation and soil – with a BRDF database*. Wissenschaft und Technik Verlag, Berlin, 2004.
- [9] ITRES Research Ltd., *Compact Airborne Spectrographic Imager CASI-1500*, 2008, <http://www.itres.com/assets/pdf/CASI-1500.pdf>.
- [10] Specim Oy/Spectral Imaging Ltd, *Airborne Hyperspectral Imaging System*, 2011, <http://www.specim.fi/products/aisa-airborne-hyperspectral-systems/aisa-series.html>.
- [11] G. Vane, R. O. Green, T. G. Chrien, H. T. Enmark, E. G. Hansen, and W. M. Porter, “The airborne visible/infrared imaging spectrometer (AVIRIS)”, *Remote Sensing of Environment*, vol. 44, no. 2–3, pp. 127–143, 1993.
- [12] A. Fernández-Renau, J. A. Gómez, and E. de Miguel, “The INTA AHS system”, in *Proceedings of the Sensors, Systems, and Next-Generation Satellites IX*, (Proc. SPIE 5978), Bruges, Belgium, 19–22 September 2005, p. 572.

- [13] D. W. Deering and P. Leone, “A sphere-scanning radiometer for rapid directional measurements of sky and ground radiance”, *Remote Sensing of Environment*, vol. 19, no. 1, pp. 1–24, 1986.
- [14] R. Leuning, D. Hughes, P. Daniel, N. C. Coops, and G. Newnham, “A multi-angle spectrometer for automatic measurement of plant canopy reflectance spectra”, *Remote Sensing of Environment*, vol. 103, no. 3, pp. 236–245, 2006.
- [15] Xsens Technologies B.V., *Magnetic field mapper, MT manager add-on. User manual*. Enschede, Netherlands, 2008.
- [16] A. Kuusk and T. Nilson, “A directional multispectral forest reflectance model”, *Remote Sensing of Environment*, vol. 72, no. 2, pp. 244–252, 2000.
- [17] A. Kuusk, J. Kuusk, M. Lang, T. Lük, and T. Nilson, “Hyperspectral reflectance of sub-boreal forests measured by CHRIS/PROBA and airborne spectrometer”, in *Proceedings of the Envisat symposium*, (ESA SP-636, CDROM), Montreux, Switzerland, 23–27 April 2007.
- [18] Carl Zeiss Jena GmbH, *MMS - monolithic miniature-spectrometer*, 2002, http://www.tec5.com/downloads/datasheets/Zeiss_modules/ZEISS_PR_MMS_engl.pdf.
- [19] Tec5 AG, *Front end electronics for NMOS spectral sensors and PDAs*, 2006, http://www.tec5.com/downloads/datasheets/technical%20datasheets/ds_fee-hs_e.pdf.
- [20] R. E. Kalman, “A new approach to linear filtering and prediction problems”, *Transactions of the ASME—Journal of Basic Engineering*, vol. 82, Series D, pp. 35–45, 1960.
- [21] Carl Zeiss Jena GmbH, *Plane grating spectrometer NIR-PGS 1.7. Product information*, 2005, http://www.tec5.com/downloads/datasheets/Zeiss_modules/pgs-nir_1_7_e.pdf.
- [22] Tec5 AG, *Temperature controller module for peltier-cooled detector arrays*, 2006, http://www.tec5.com/downloads/datasheets/technical%20datasheets/ds_PELTIER-tc_e.pdf.
- [23] E. Dereniak and D. Crowe, *Optical radiation detectors*. New York, US: John Wiley & Sons, Inc., 1984, p. 300.
- [24] Carl Zeiss Jena GmbH, *Plane grating spectrometer NIR-PGS 2.2. Product information*, 2005, http://www.tec5.com/downloads/datasheets/Zeiss_modules/pgs-nir_2_2_e.pdf.
- [25] P. Huber, OEM components product manager, Tec5 AG, In der Au 27, 61440 Oberursel, Germany (personal communication), 2009.

- [26] V. A. Nikitin, “Spectral-instrument manufacture in the USSR”, *Journal of Applied Spectroscopy*, vol. 12, no. 4, pp. 439–448, 1970.
- [27] É. I. Terez, “The instrumental characteristics of monochromators”, *Journal of Applied Spectroscopy*, vol. 19, no. 4, pp. 1340–1343, 1973.
- [28] H. Kostkowski, *Reliable spectroradiometry*. La Plata, Md.: Spectroradiometry Consulting, 1997, p. 609.
- [29] P. Deschamps, F. Bréon, M. Leroy, A. Podaire, A. Bricaud, J. Buriez, and G. Sèze, “The POLDER mission - instrument characteristics and scientific objectives”, *IEEE Transactions on Geoscience and Remote Sensing*, vol. 32, no. 3, pp. 598–615, 1994.
- [30] VALERI, *VALidation of Land European Remote sensing Instruments*, 2008, <http://w3.avignon.inra.fr/valeri/>.
- [31] RAMI, *RAdiation transfer Model Intercomparison*, 2009, <http://rami-benchmark.jrc.ec.europa.eu/HTML/RAMI-IV/RAMI-IV.php>.
- [32] A. Kuusk, M. Lang, and T. Nilson, “Forest test site at Järvelja, Estonia”, in *Proceedings of the 3rd ESA CHRIS/Proba Workshop*, (ESA SP-593, CDROM), ESRIN, Frascati, Italy, 21–23 March 2005, pp. 1–7.
- [33] A. Kuusk, M. Lang, J. Kuusk, T. Lükk, T. Nilson, M. Möttus, M. Rautiainen, and A. Eenmäe, “Database of optical and structural data for the validation of radiative transfer models”, Tartu Observatory, Estonia, Tech. Rep., 2009, p. 58, http://www.aai.ee/bgf/jarvelja_db/jarvelja_db.pdf.
- [34] M. Lang, A. Kuusk, T. Nilson, T. Lükk, M. Pehk, and G. Alm, *Reflectance spectra of ground vegetation in sub-boreal forests*, 2002, <http://www.aai.ee/bgf/ger2600/>.
- [35] H. Erives, X. Xiong, J. Sun, J. Esposito, S. Xiong, and W. Barnes, “Terra MODIS RSB on-orbit calibration and performance: four years of data”, in *Proceedings of the Sensors, Systems, and Next-Generation Satellites VII*, (Proc. SPIE 5570), Maspalomas, Gran Canaria, Spain, 13–15 September 2004, p. 342.
- [36] J. Liu, Z. Li, Y. Qiao, Y. Liu, and Y. Zhang, “A new method for cross-calibration of two satellite sensors”, *International Journal of Remote Sensing*, vol. 25, no. 23, pp. 5267–5281, 2004.
- [37] N. Leisso, K. Thome, and J. Czapla-Myers, “Validation of the onboard radiometric calibration of the GOES I-M visible channel by reflectance-based vicarious methods”, in *Proceedings of the Atmospheric and environmental remote sensing data processing and utilization III*, (Proc. SPIE 6684), San Diego, California, USA, 27–28 and 30 August 2007, pp. 668404.1–668404.10.

- [38] N. Chrien, C. Bruegge, and R. Ando, “Multi-angle imaging spectroradiometer (MISR) on-board calibrator (OBC) in-flight performance studies”, *IEEE Transactions on Geoscience and Remote Sensing*, vol. 40, no. 7, pp. 1493–1499, 2002.
- [39] M. Dinguirard and P. Slater, “Calibration of space-multispectral imaging sensors: a review”, *Remote Sensing of Environment*, vol. 68, no. 3, pp. 194–205, 1999.
- [40] B. Horn and R. Woodham, *Destriping satellite images*. Massachusetts Institute of Technology, A.I. Memo No. 467, 1978.
- [41] A. Kuusk, “Monitoring of vegetation parameters on large areas by the inversion of a canopy reflectance model”, *International Journal of Remote Sensing*, vol. 19, no. 15, pp. 2893–2905, 1998.
- [42] M. Banham and A. Katsaggelos, “Digital image restoration”, *IEEE Signal Processing Magazine*, vol. 14, no. 2, pp. 24–41, 1997.
- [43] C. Podilchuk, “Signal recovery from partial information”, in *The Digital Signal Processing Handbook*, V. Madisetti and D. Williams, Eds., Boca Raton, Florida: CRC Press LLC, 1998,
- [44] S. Liang, *Quantitative Remote Sensing of Land Surfaces*. Hoboken, New Jersey: Wiley-Interscience, 2004, p. 534.
- [45] W. Abdou, C. Bruegge, M. Helmlinger, J. Conel, S. Pilorz, W. Ledebor, B. Gaitley, and K. Thome, “Vicarious calibration experiment in support of the multi-angle imaging spectroradiometer”, *IEEE Transactions on Geoscience and Remote Sensing*, vol. 40, no. 7, pp. 1500–1511, 2002.
- [46] M. Cutter, “Review of aspects associated with the CHRIS calibration”, in *Proceedings of the 2nd CHRIS/Proba workshop*, (ESA SP-578, CDROM), ESRIN, Frascati, Italy, 21–23 March 2004.
- [47] U. Peterson and T. Nilson, “Successional reflectance trajectories in northern temperate forests”, *International Journal of Remote Sensing*, vol. 14, no. 3, pp. 609–613, 1993.
- [48] T. Nilson and U. Peterson, “Age dependence of forest reflectance - analysis of main driving factors”, *Remote Sensing of Environment*, vol. 48, no. 3, pp. 319–331, 1994.
- [49] M. Russelle, W. Wilhelm, R. Olson, and J. Power, “Growth analysis based on degree days”, *Crop Science*, vol. 24, no. Jan.-Feb., pp. 28–32, 1984.
- [50] S. Jacquemoud and F. Baret, “PROSPECT: a model of leaf optical properties spectra”, *Remote Sensing of Environment*, vol. 34, no. 2, pp. 75–91, 1990.

- [51] H. W. Gausman, W. A. Allen, R. Cardenas, and A. J. Richardson, “Effects of leaf nodal position on absorption and scattering coefficients and infinite reflectance of cotton leaves, *Gossypium hirsutum* l.1”, *Agronomy Journal*, vol. 63, no. 1, pp. 87–91, 1971.
- [52] A. Kuusk, “A two-layer canopy reflectance model”, *Journal of Quantitative Spectroscopy & Radiative Transfer*, vol. 71, no. 1, pp. 1–9, 2001.
- [53] J.-L. Widlowski, M. Taberner, B. Pinty, V. Bruniquel-Pinel, M. Disney, R. Fernandes, J.-P. Gastellu-Etchegorry, N. Gobron, A. Kuusk, T. Lavergne, S. Leblanc, P. E. Lewis, E. Martin, M. Möttus, P. R. J. North, W. Qin, M. Robustelli, N. Rochdi, R. Ruiloba, C. Soler, R. Thompson, W. Verhoef, M. M. Verstraete, and D. Xie, “Third radiation transfer model intercomparison (RAMI) exercise: documenting progress in canopy reflectance models”, *Journal of Geophysical Research*, vol. 112, no. D091111, pp. 1–28, 2007.

SUMMARY IN ESTONIAN

Metsade atmosfääriluse spektraalse peegelduskoefitsiendi mõõtmine taimkatte kiirguslevimudelite arendamiseks

Taimestik mõjutab kogu ökosüsteemi ja kliimat. Selle uurimine ja jälgimine on seetõttu olnud läbi aegade kaugseire üks olulisemaid valdkondi. Kaugseiresatelliitide levik 20. sajandi teisest poolest alates on oluliselt laiendanud kaugseire võimalusi. Satelliidilt on korraga näha väga suur ala ja sobivate ilmastikutingimuste korral on võimalik lihtsa vaevaga teha kordusmõõtmisi. Et mõõdetud andmetest mingit sisulist infot eraldada, on vaja aru saada, kuidas mõõdetav signaal moodustub ja mis seda mõjutab. Taimkatte kiirguslevimudelid hõlmavadki endas seda teadmiste baasi. Nad võimaldavad arvutada, kuidas metsale langev päikesekiirgus neeldub ja hajub olenevalt taimkatte struktuurist ja optilistest omadustest.

Mudelite arendamiseks on vaja mõõtmistulemusi reaalsest elust, et neid saaks võrrelda modelleeritud andmetega ning erinevuse korral mudelit parandada. Satelliidilt mõõdetud signaal läbib sensori ja objekti vahele jääva atmosfäärikihi, mis moonutab signaali. Seetõttu saab kõige parema tulemuse mõõtes metsalt hajunud päikesekiirgust võimalikult madalalt metsa kohal, et objekti ja sensori vahele jääv atmosfäärikiht mõjutaks signaali tühiselt vähe. Samuti saab atmosfääriluste mõõtmiste abil kontrollida ja vajadusel parandada satelliidipildi atmosfäärikorrektsiooni ja sensori kalibratsioonikoefitsiente.

Maailmas on sooritatud palju metsade lennukimõõtmisi erinevate instrumentidega, aga need on kõik tehtud kõrgemal kui 500 m. Vahetult metsa kohal on metsa peegelduskoefitsiendi mõõdetud metsast kõrgemate mastide külge kinnitatud mõõteriistadega, aga need näevad vaid väga piiratud maa-ala. Käesoleva töö eesmärgiks oli välja töötada ning valmistada sobilik aparaat metsade atmosfääriluse spektraalse peegelduskoefitsiendi mõõtmiseks ja reaalsete mõõtmiste läbiviimiseks.

Töö käigus on valminud spektromeetrite seeria UAVSpec [I]. Alates 2006. aastast on igal suvel Eesti Maaülikooli Järvelja Katse- ja Õppemetskonnas mõõdetud Robinson R22 helikopterilt metsade spektraalset heledust. Algusest peale on silmas peetud võimalust kasutada UAVSpec spektromeetrite kandurina mehita mata lennuvahendit, mistõttu on spektromeetrid disainitud täisautonoomsed ning piisavalt väiksed ja kerged.

Suurus ja kaal seavad piirid kasutatavatele komponentidele. Kasutatud on Zeiss Jena GmbH poolt toodetud minispektromeetrite mooduleid. Paraku on väiksed mõõtmised saavutatavad optilise kvaliteedi arvelt. Ühtlasi pole tegu valmis spektromeetritega, seega metrooloogiliselt oluliste omaduste parametrizeerimine on jäetud mooduli kasutaja hooleks. Laborimõõtmiste põhjal parametrizeeriti spektromeetri

pimevoolu sõltuvus temperatuurist ning integreerimisajast [III]. Mõõdeti hajuvallguse ja spektraalse läbikostvuse poolt tekitatud vead. Koostati algoritmid registreeritud signaalide radiomeetriliseks korrektsiooniks.

Taimkatte kiirguslevimudelid vajavad väga suurt hulka sisendparameetreid, mida tavapärase metsa takseerimise käigus ei mõõdetata. Seetõttu koostati mahukas andmekogum kolme Järvelja puistu kohta [III]. Nendeks olid 1 ha pindalaga kuusik, männik ja kaasik. Neist männikut ja kaasikut kasutati rahvusvahelise taimkatte kiirguslevimudelite võrdluskatse RAMI neljandas faasis testobjektide defineerimiseks. Tegu oli esimese korraga, kui RAMI võrdlustes kasutati objektideks reaalseid puistuid. UAVSpec seeria spektrometritega sooritatud metsa ning alustaimestiku heleduse mõõtmised olid andmebaasi koostamisel olulise tähtsusega.

10.07.2005 mõõtis Euroopa Kosmoseagentuuri eksperimentaalsatelliidil PROBA paiknev kujutise spektromeeter CHRIS Järvelja piirkonda. Kahjuks valmis esimene UAVSpec seeria spektromeeter alles 2006. a. suveks, mistõttu oli võimalik võrrelda vaid aastase vahega, kuid siiski vegetatsiooniperioodi samas faasis sooritatud mõõtmisi. Nende tulemuste alusel pakuti välja põhjalik protsessikirjeldus satelliidipiltide töötlemiseks ja satelliitsensorite kalibratsiooniks [IV]. Kuigi leitud parandid CHRISi kaliibrimiskordajate jaoks ei pruugi eelmainitud aastase erinevuse tõttu olla kõige usaldusväärsemad, võib sama korrektsiooniprotsessi kasutada tulevikus toimuvate samaaegsete mõõtmiste võrdlemiseks.

Väga erinev sademete hulk järjestikustel aastatel 2006 ja 2007 andis võimaluse uurida täiskasvanud metsa spektraalse peegelduskoeffitsiendi sõltuvust sademete hulgast. Neil aastail sooritatud kopterimõõtmiste hulgast selekteeriti välja need puistud, mis olid piisavalt suured ning homogeensed ja mida mõõdeti mõlemal aastal. Tulemused näitavad, et kuigi täiskasvanud metsa heledust on senimaani peetud pikas perspektiivis stabiilseks, võib aastast aastasse muutus sõltuvalt puuliigist ja spektripiirkonnast ulatuda isegi üle 20% [V].

Tartu Observatooriumis väljatöötatud metsa peegeldusmudeliga FRT simuleeriti kolme andmebaasis kirjeldatud puistu peegeldusspektreid ning võrreldi neid reaalseste mõõtmistulemustega [VI]. Võrdluse käigus selgus, et mudel ilmselt eksib taimkattes ja maapinnal varjude tõenäosuse arvutamise ja probleemid peegeldusteguri modelleerimisel lähedase infrapunase piirkonnas viitavad võimalikele vigadele mitmekordse hajumise käsitlemisel. Taas jõuti ka modelleerimise põhitõeni, et mudeli väljundandmete täpsuse määrab suuresti sisendparameetrite täpsus.

ACKNOWLEDGMENTS

I wish to thank the Tartu Observatory for providing me an interesting topic, warm and helpful colleagues, and all the necessary resources for this study. I am grateful to my father and supervisor Andres Kuusk who has always helped me in the lab with discussing different problems as well as on the field carrying out measurements. He has helped me to shape this thesis and all the papers to their final form. The valuable comments on this thesis by my other supervisor Mart Noorma are greatly appreciated.

I wish to thank the Archimedes foundation for the Kristjan Jaak travel grant. I also want to express my sincerest gratitude to the OÜ Pakker Avio for providing the helicopter for numerous test flights and field campaigns, and especially to their excellent pilot Romet Vään. Many thanks go to Mait Lang for being the navigator during every single airborne measurement campaign.

This study was supported by

- Estonian Science Foundation grants Nos. 6100, 6812, and 7725.
- Estonian Ministry of Education and Research target-financed projects Nos. SF0062466s03, SF0060115s08, and SF0180009Bs11.
- European Union Seventh Framework Programme Capacities project EstSpace
- Doctoral School of Ecology and Environmental Sciences.
- Doctoral School of Earth Sciences and Ecology.
- Centre of Excellence on Theoretical and Applied Ecology.

PUBLICATIONS

CURRICULUM VITAE

General information

Name: Joel Kuusk
Date and place of birth: 29 July 1981, Tartu
Citizenship: Estonian
Address: Tartu Observatory
61602, Tõravere
Tartumaa
Estonia
E-mail: joel@aai.ee

Educational history:

1988–1999 Miina Härma Gymnasium, Tartu
1999–2003 University of Tartu, BSc in physics (*cum laude*)
2003–2005 University of Tartu, MSc in physics (applied physics)
2005–2011 University of Tartu, PhD studies in physics (applied physics)

Languages spoken: Estonian, English

Professional employment:

2001–2002 Tartu Observatory, contractual worker
2006–2010 Tartu Observatory, engineer
2011– Tartu Observatory, research associate

Scientific and research activity

Main research interests: vegetation remote sensing, optical radiometry

Publications indexed by ISI Web of Science:

- [1] M. Rautiainen, M. Lang, M. Möttus, A. Kuusk, T. Nilson, J. Kuusk, and T. Lükk, “Multi-angular reflectance properties of a hemiboreal forest: an analysis using CHRIS PROBA data”, *Remote Sensing of Environment*, vol. 112, no. 5, pp. 2627–2642, 2008.
- [2] A. Kuusk, T. Nilson, M. Paas, M. Lang, and J. Kuusk, “Validation of the forest radiative transfer model FRT”, *Remote Sensing of Environment*, vol. 112, no. 1, pp. 51–58, 2008.
- [3] A. Kuusk, J. Kuusk, and M. Lang, “A dataset for the validation of reflectance models”, *Remote Sensing of Environment*, vol. 113, no. 5, pp. 889–892, 2009.

- [4] J. Kuusk, A. Kuusk, M. Lang, and A. Kallis, “Hyperspectral reflectance of boreo-nemoral forests in a dry and normal summer”, *International Journal of Remote Sensing*, vol. 31, no. 1, pp. 159–175, 2010.
- [5] A. Kuusk, T. Nilson, J. Kuusk, and M. Lang, “Reflectance spectra of RAMI forest stands in Estonia : simulations and measurements”, *Remote Sensing of Environment*, vol. 114, no. 12, pp. 2962–2969, 2010.

Scholarships:

- Juhan Ross scholarship, Tartu Observatory, 2005
- Kristjan Jaak travel grant, Archimedes foundation, 2009

Further professional training

International courses attended:

- ”Physical Models in Remote Sensing”, Tikkurila, Finland, 13–14 April 2004
- ”Tree canopy structure and functioning from below and above”, Järvelja, Estonia, 3–14 September 2006

ELULOOKIRJELDUS

Üldandmed

Ees- ja perekonnanimi: Joel Kuusk
Sünniaeg ja koht: 29.07.1981, Tartu
Kodakondsus: Eesti
Aadress: Tartu Observatoorium
61602, Tõravere
Tartumaa
Eesti
E-post: joel@aai.ee

Hariduskäik:

1988–1999 Miina Härma Gümnaasium, Tartu
1999–2003 Tartu Ülikool, BSc füüsika erialal (*cum laude*)
2003–2005 Tartu Ülikool, MSc füüsika erialal (rakendusfüüsika)
2005–2011 Tartu Ülikool, doktorantuur füüsika erialal (rakendusfüüsika)

Keelteoskus: eesti, inglise

Teenistuskäik:

2001–2002 Tartu Observatoorium, lepinguline töötaja
2006–2010 Tartu Observatoorium, insener
2011– Tartu Observatoorium, teadur

Teaduslik ja arendustegevus

Peamised uurimisvaldkonnad: taimkatte kaugseire, optiline radiomeetria

ISI Web of Science andmebaasis kajastatud publikatsioonide loetelu:

- [1] M. Rautiainen, M. Lang, M. Möttö, A. Kuusk, T. Nilson, J. Kuusk ja T. Lükk, “Multi-angular reflectance properties of a hemiboreal forest: an analysis using CHRIS PROBA data”, *Remote Sensing of Environment*, kd. 112, nr. 5, lk. 2627–2642, 2008.
- [2] A. Kuusk, T. Nilson, M. Paas, M. Lang ja J. Kuusk, “Validation of the forest radiative transfer model FRT”, *Remote Sensing of Environment*, kd. 112, nr. 1, lk. 51–58, 2008.
- [3] A. Kuusk, J. Kuusk ja M. Lang, “A dataset for the validation of reflectance models”, *Remote Sensing of Environment*, kd. 113, nr. 5, lk. 889–892, 2009.
- [4] J. Kuusk, A. Kuusk, M. Lang ja A. Kallis, “Hyperspectral reflectance of boreo-nemoral forests in a dry and normal summer”, *International Journal of Remote Sensing*, kd. 31, nr. 1, lk. 159–175, 2010.

- [5] A. Kuusk, T. Nilson, J. Kuusk ja M. Lang, “Reflectance spectra of RAMI forest stands in Estonia : simulations and measurements”, *Remote Sensing of Environment*, kd. 114, nr. 12, lk. 2962–2969, 2010.

Saadud uurimistoetused ja stipendiumid:

- Juhan Rossi stipendium, Tartu Observatoorium, 2005
- Kristjan Jaagu välislähetuse stipendium, SA Archimedes, 2009

Erialane enesetäiendus

Osalemine rahvusvahelistel kraadiõppe-kursustel:

- ”Physical Models in Remote Sensing”, Tikkurila, Soome, 13–14 aprill 2004
- ”Tree canopy structure and functioning from below and above”, Järvelja, Eesti, 3–14 september 2006

DISSERTATIONES PHYSICAE UNIVERSITATIS TARTUENSIS

1. **Andrus Ausmees.** XUV-induced electron emission and electron-phonon interaction in alkali halides. Tartu, 1991.
2. **Heiki Sõnajalg.** Shaping and recalling of light pulses by optical elements based on spectral hole burning. Tartu, 1991.
3. **Sergei Savihhin.** Ultrafast dynamics of F-centers and bound excitons from picosecond spectroscopy data. Tartu, 1991.
4. **Ergo Nõmmiste.** Leelishalogeniidide röntgenelektronemissioon kiiritamisel footonitega energiaga 70–140 eV. Tartu, 1991.
5. **Margus Rätsep.** Spectral gratings and their relaxation in some low-temperature impurity-doped glasses and crystals. Tartu, 1991.
6. **Tõnu Pullerits.** Primary energy transfer in photosynthesis. Model calculations. Tartu, 1991.
7. **Olev Saks.** Attoampri diapsoonis voolude mõõtmise füüsikalised alused. Tartu, 1991.
8. **Andres Virro.** AlGaAsSb/GaSb heterostructure injection lasers. Tartu, 1991.
9. **Hans Korge.** Investigation of negative point discharge in pure nitrogen at atmospheric pressure. Tartu, 1992.
10. **Jüri Maksimov.** Nonlinear generation of laser VUV radiation for high-resolution spectroscopy. Tartu, 1992.
11. **Mark Aizengendler.** Photostimulated transformation of aggregate defects and spectral hole burning in a neutron-irradiated sapphire. Tartu, 1992.
12. **Hele Siimon.** Atomic layer molecular beam epitaxy of A^2B^6 compounds described on the basis of kinetic equations model. Tartu, 1992.
13. **Tõnu Reinot.** The kinetics of polariton luminescence, energy transfer and relaxation in anthracene. Tartu, 1992.
14. **Toomas Rõõm.** Paramagnetic H^{2-} and F^+ centers in CaO crystals: spectra, relaxation and recombination luminescence. Tallinn, 1993.
15. **Erko Jalviste.** Laser spectroscopy of some jet-cooled organic molecules. Tartu, 1993.
16. **Alvo Aabloo.** Studies of crystalline celluloses using potential energy calculations. Tartu, 1994.
17. **Peeter Paris.** Initiation of corona pulses. Tartu, 1994.
18. **Павел Рубин.** Локальные дефектные состояния в CuO_2 плоскостях высокотемпературных сверхпроводников. Тарту, 1994.
19. **Olavi Ollikainen.** Applications of persistent spectral hole burning in ultrafast optical neural networks, time-resolved spectroscopy and holographic interferometry. Tartu, 1996.
20. **Ülo Mets.** Methodological aspects of fluorescence correlation spectroscopy. Tartu, 1996.
21. **Mikhail Danilkin.** Interaction of intrinsic and impurity defects in CaS:Eu luminophors. Tartu, 1997.

22. **Ирина Кудрявцева.** Создание и стабилизация дефектов в кристаллах KBr, KCl, RbCl при облучении ВУФ-радиацией. Тарту, 1997.
23. **Andres Osvet.** Photochromic properties of radiation-induced defects in diamond. Tartu, 1998.
24. **Jüri Örd.** Classical and quantum aspects of geodesic multiplication. Tartu, 1998.
25. **Priit Sarv.** High resolution solid-state NMR studies of zeolites. Tartu, 1998.
26. **Сергей Долгов.** Электронные возбуждения и дефектообразование в некоторых оксидах металлов. Тарту, 1998.
27. **Кауро Кукли.** Atomic layer deposition of artificially structured dielectric materials. Tartu, 1999.
28. **Ivo Heinmaa.** Nuclear resonance studies of local structure in $\text{RBa}_2\text{Cu}_3\text{O}_{6+x}$ compounds. Tartu, 1999.
29. **Aleksander Shelkan.** Hole states in CuO_2 planes of high temperature superconducting materials. Tartu, 1999.
30. **Dmitri Nevedrov.** Nonlinear effects in quantum lattices. Tartu, 1999.
31. **Rein Ruus.** Collapse of 3d (4f) orbitals in 2p (3d) excited configurations and its effect on the x-ray and electron spectra. Tartu, 1999.
32. **Valter Zazubovich.** Local relaxation in incommensurate and glassy solids studied by Spectral Hole Burning. Tartu, 1999.
33. **Indrek Reimand.** Picosecond dynamics of optical excitations in GaAs and other excitonic systems. Tartu, 2000.
34. **Vladimir Babin.** Spectroscopy of exciton states in some halide macro- and nanocrystals. Tartu, 2001.
35. **Toomas Plank.** Positive corona at combined DC and AC voltage. Tartu, 2001.
36. **Kristjan Leiger.** Pressure-induced effects in inhomogeneous spectra of doped solids. Tartu, 2002.
37. **Helle Kaasik.** Nonperturbative theory of multiphonon vibrational relaxation and nonradiative transitions. Tartu, 2002.
38. **Tõnu Laas.** Propagation of waves in curved spacetimes. Tartu, 2002.
39. **Rünno Lõhmus.** Application of novel hybrid methods in SPM studies of nanostructural materials. Tartu, 2002.
40. **Kaido Reivelt.** Optical implementation of propagation-invariant pulsed free-space wave fields. Tartu, 2003.
41. **Heiki Kasemägi.** The effect of nanoparticle additives on lithium-ion mobility in a polymer electrolyte. Tartu, 2003.
42. **Villu Repän.** Low current mode of negative corona. Tartu, 2004.
43. **Алексей Котлов.** Оксианионные диэлектрические кристаллы: зонная структура и электронные возбуждения. Тарту, 2004.
44. **Jaak Talts.** Continuous non-invasive blood pressure measurement: comparative and methodological studies of the differential servo-oscillometric method. Tartu, 2004.
45. **Margus Saal.** Studies of pre-big bang and braneworld cosmology. Tartu, 2004.

46. **Eduard Gerškevičš.** Dose to bone marrow and leukaemia risk in external beam radiotherapy of prostate cancer. Tartu, 2005.
47. **Sergey Shchemel'ov.** Sum-frequency generation and multiphoton ionization in xenon under excitation by conical laser beams. Tartu, 2006.
48. **Valter Kiisk.** Optical investigation of metal-oxide thin films. Tartu, 2006.
49. **Jaan Aarik.** Atomic layer deposition of titanium, zirconium and hafnium dioxides: growth mechanisms and properties of thin films. Tartu, 2007.
50. **Astrid Rekker.** Colored-noise-controlled anomalous transport and phase transitions in complex systems. Tartu, 2007.
51. **Andres Punning.** Electromechanical characterization of ionic polymer-metal composite sensing actuators. Tartu, 2007.
52. **Indrek Jõgi.** Conduction mechanisms in thin atomic layer deposited films containing TiO₂. Tartu, 2007.
53. **Aleksei Krasnikov.** Luminescence and defects creation processes in lead tungstate crystals. Tartu, 2007.
54. **Küllike Rägo.** Superconducting properties of MgB₂ in a scenario with intra- and interband pairing channels. Tartu, 2008.
55. **Els Heinsalu.** Normal and anomalously slow diffusion under external fields. Tartu, 2008.
56. **Kuno Kooser.** Soft x-ray induced radiative and nonradiative core-hole decay processes in thin films and solids. Tartu, 2008.
57. **Vadim Boltrushko.** Theory of vibronic transitions with strong nonlinear vibronic interaction in solids. Tartu, 2008.
58. **Andi Hektor.** Neutrino Physics beyond the Standard Model. Tartu, 2008.
59. **Raavo Josepson.** Photoinduced field-assisted electron emission into gases. Tartu, 2008.
60. **Martti Pärs.** Study of spontaneous and photoinduced processes in molecular solids using high-resolution optical spectroscopy. Tartu, 2008.
61. **Kristjan Kannike.** Implications of neutrino masses. Tartu, 2008.
62. **Vigen Issahhanjan.** Hole and interstitial centres in radiation-resistant MgO single crystals. Tartu, 2008.
63. **Veera Krasnenko.** Computational modeling of fluorescent proteins. Tartu, 2008.
64. **Mait Müntel.** Detection of doubly charged higgs boson in the CMS detector. Tartu, 2008.
65. **Kalle Kepler.** Optimisation of patient doses and image quality in diagnostic radiology. Tartu, 2009.
66. **Jüri Raud.** Study of negative glow and positive column regions of capillary HF discharge. Tartu, 2009.
67. **Sven Lange.** Spectroscopic and phase-stabilisation properties of pure and rare-earth ions activated ZrO₂ and HfO₂. Tartu, 2010.
68. **Aarne Kasikov.** Optical characterization of inhomogeneous thin films. Tartu, 2010.

69. **Heli Valtna-Lukner.** Superluminally propagating localized optical pulses. Tartu, 2010.
70. **Artjom Vargunin.** Stochastic and deterministic features of ordering in the systems with a phase transition. Tartu, 2010.
71. **Hannes Liivat.** Probing new physics in e^+e^- annihilations into heavy particles via spin orientation effects. Tartu, 2010.
72. **Tanel Mullari.** On the second order relativistic deviation equation and its applications. Tartu, 2010.
73. **Aleksandr Lisovski.** Pulsed high-pressure discharge in argon: spectroscopic diagnostics, modeling and development. Tartu, 2010.
74. **Aile Tamm.** Atomic layer deposition of high-permittivity insulators from cyclopentadienyl-based precursors. Tartu, 2010.
75. **Janek Uin.** Electrical separation for generating standard aerosols in a wide particle size range. Tartu, 2011.
76. **Svetlana Ganina.** Hajusandmetega ülesanded kui üks võimalus füüsika-õppe efektiivsuse tõstmiseks. Tartu, 2011